Applied Thermal Engineering 244 (2024) 122666

Contents lists available at ScienceDirect

Applied Thermal Engineering

journal homepage: www.elsevier.com/locate/apthermeng

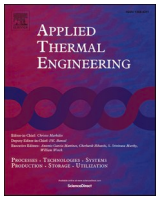

Research Paper

Development of compact empirical models for variable-speed compressors for the prediction of energy consumption, mass flow and discharge temperature

Rubén Ossorio *, Javier Marchante-Avellaneda, Emilio Navarro-Peris

Instituto Universitario de Investigación en Ingeniería Energética (IUIIE), Universitat Politècnica de València, Camino de Vera s/n, ed. 8E cubo F 5° 46022, Valencia, Spain

ARTICLE INFO

Keywords:
Variable speed compressor
Modeling
Consumption
Mass flow
Discharge temperature

ABSTRACT

In the context of heat pumps, developing prediction models for compressor performance holds significant importance for design, selection, control, and fault detection. Nevertheless, there is not currently an established standard for characterizing variable-speed compressors. Various published models offer different advantages and trade-offs in terms of accuracy and simplicity however, none of them strike the right balance between complexity and data fidelity, which is paramount, especially when working with limited or low-fidelity data.

This study conducts a detailed analysis on how the compressor performance evolves within the compressor envelope focusing on the speed effect and, from this analysis, novel compact empirical models are obtained to predict mass flow rate and energy consumption. A study of discharge temperature is also presented in this work due to its relevance in quantifying heating capacity and power losses. To model it, a correlation based on electro-mechanical efficiency is proposed, which can be generalized for different suction conditions without introducing additional coefficients. The proposed models are data-driven by high-fidelity calorimetric tests and aim to maintain simplicity, using no more than six coefficients, while delivering acceptable accuracy with average prediction errors lower than 5%. Finally, a robustness analysis is carried out, which analyzes the required training data needed to fit the model and concludes that the proposed models can compete in accuracy with models that use much more coefficients.

1. Introduction

System modeling, particularly in the domain of HVAC systems, has become increasingly important due to a rapidly changing regulatory environment that places greater emphasis on mitigating climate change and global warming. Compressors play a critical role in HVAC systems, and accurately predicting their performance is essential for optimizing energy efficiency and reducing environmental impact.

Modeling approaches can be broadly categorized as either detailed models (white-box), empirical models (black-box) and semi-empirical models (grey-box). While all approaches have their merits, the choice of modeling approach depends on the available data, computational resources, desired accuracy and final application. White-box models, which are based on fundamental physical principles, provide detailed insights into the underlying physical phenomena but are more computationally intensive, are less integrable and require extensive knowledge of the system which is typically unavailable (utilized mainly by component designers and manufacturers). Grey-box models are formulated using equations describing physical processes and use experimental data to fit parameters such as polytropic coefficients, heat transfer coefficients, death volumes, etc. Their accuracy is limited and related to the assumptions taken. They typically involve fitting exponents or solving complex equations, making them harder to fit for general users and more challenging to implement in bigger simulation systems. In contrast, black-box or empirical models only rely on data-driven relationships, and although they may lack physical interpretability, they offer simplicity and flexibility by capturing the observed behavior of the system.

Manufacturers commonly have used a black-box model for characterizing fixed-speed compressors (standard AHRI-540 [1]). The standard defines a third-degree polynomial expression with 10 fitting coefficients for predicting energy consumption and mass flow rate as a function of evaporating and condensing temperatures. Nevertheless, this standard is

* Corresponding author.
E-mail address: r.ossorio@iie.upv.es (R. Ossorio).

https://doi.org/10.1016/j.applthermaleng.2024.122666
Received 10 November 2023; Received in revised form 10 January 2024; Accepted 5 February 2024
Available online 15 February 2024

Nomenclature

Abbreviations

CV	coefficient of variance of RMSE
displ	compressor displacement
PR	Pressure Ratio
RMSE	Root Mean Square Error

Symbols

f_c	compressor speed [Hz]
$k_{\#}$,$s_{\#}$,$c_{\#}$	fitting coefficients
k_c	compressor efficiency ratio
k_m	mass flow ratio
k_p	consumption ratio
k_v	volumetric efficiency ratio
$\dot{m}$	mass flow [g/s]
P	pressure [bar]
SH	Super Heat [K]
T	temperature [K]
$\dot{W}_c$	compressor consumption [W]
$\bar{X}$	Magnitude average

Subindex

0	at no load
1	suction
2	discharge
c	condensing
e	evaporating
esp	specific (divided by $\dot{m}$)
is	isentropic
nom	at reference speed
pred	predicted with a prefitted correlation
rat	ratio with nominal conditions

Superindex

#	at reference SH
‘	Redefined

Greek letters

α	loss fraction of effective work
η_c	compressor efficiency
η_{em}	electromechanical efficiency
η_{is}	isentropic efficiency
η_v	volumetric efficiency
ρ	density [kg/m^3]

becoming outdated today because heat pump and chiller manufacturers are now moving to use variable-speed compressors, where the compressor speed plays a key role in its performance.

Unfortunately, there is currently no established standard for characterizing variable-speed compressors, and a common solution adopted by manufacturers is to use a similar approach to the one described in the AHRI-540 but introducing the speed as an extra independent variable [2–5]. This results in a total of 20 terms considering a second-order polynomial and three independent variables (T_e, T_c and f_c) [Eq.(1)]. This model will be called AHRI-20 from now on.

$$\begin{aligned}\dot{m}|\dot{W}_c = {} & k_1 + k_2T_e + k_3T_c + k_4f_c + k_5T_e^2 + k_6T_c^2 + k_7f_c^2 + k_8T_eT_c + k_9T_ef_c \\ & + k_{10}T_cf_c + k_{11}T_e^3 + k_{12}T_c^3 + k_{13}f_c^3 + k_{14}T_e^2T_c + k_{15}T_e^2f_c + k_{16}T_c^2T_e \\ & + k_{17}T_c^2f_c + k_{18}f_c^2T_e + k_{19}f_c^2T_c + d_{20}T_eT_cf_c\end{aligned} \tag{1}$$

One crucial aspect when proposing a compressor model based on experimental information (especially for black-box models) is adapting its complexity to the information embedded in the available data. If the model becomes too complex, it will start capturing noise rather than authentic underlying patterns. This behavior is called overfitting and can lead to inaccurate predictions, particularly in cases of limited or low-fidelity data. A previous study [6] highlighted the limitations of AHRI-20, the study showed that the model tended to overfit when data is scarce or lacks fidelity. To avoid such issues, it is essential to carefully select and justify the complexity of the proposed model to ensure accurate interpolation and extrapolation.

Other studies have explored the use of Artificial Neural Networks (ANNs) to model compressors [7–10]. While ANNs can capture complex relationships within the data, their integration into other systems and reporting fitted parameters can be challenging. The difficulty lies in the opaque nature of ANNs, making it difficult to interpret the underlying relationships and understand the model’s behavior. In contrast, compact linear models with justified complexity offer a promising alternative, providing acceptable accuracy while remaining transparent and interpretable.

In Ossorio and Navarro-Peris [6], the performance of the most used compact models to predict energy consumption for variable speed compressors were analyzed. In the analysis, either empirical or explicit semi-empirical models were included, and they were evaluated with a train-test procedure. Semi-empirical models performed generally well, showing an acceptable accuracy with a limited number of fitting coefficients. However, due to their non-linear formulation, they had convergence problems during coefficient fitting. Among the studied models, Shao’s model [Eq.(2)] offered a good trade-off between complexity and accuracy and managed to be applicable also to scroll compressors, even if it was originally tested only with rotary technology. However, the number of coefficients used were not analyzed. Additionally, a model for discharge temperature was not proposed, and the effect of SH on performance was not assessed.

$$\dot{m}_{nom}|\dot{W}_{c,nom} = k_1 + k_2T_e + k_3T_c + k_4T_e^2 + k_5T_c^2 + k_6T_eT_c$$

$$k_{m|p} = \frac{\dot{m}}{\dot{m}_{nom}} \; or \; \frac{\dot{W}_c}{\dot{W}_{c,nom}} = c_1\left(f_c - f_{c,nom}\right)^2 + c_2\left(f_c - f_{c,nom}\right)^2 + c_3 \tag{2}$$

Modeling discharge temperature in compressors is also vital as it provides information about power losses, heating capacity and condenser inlet temperature. However, it remains a topic of limited study compared with the proposed mass flow and energy consumption models. The most common approaches assume constant isentropic efficiencies or introduce a term dependent on energy consumption to model energy losses (e.g., Ashrae Toolkit [11]). Others try modeling ambient losses as a function of a virtual compressor shell temperature [12].

Given the introduced state of the art, this study proposes compact map-based models to predict mass flow rate, compressor energy consumption and discharge temperature with a low number of coefficients. The proposed models can also model the effect of speed on the compressor performance and show average prediction errors lower than 5 %, having no more than six fitting coefficients. Moreover, the impact of suction conditions on the modeled variables is assessed, and a general correlation is proposed to model it without introducing new fitting coefficients. Finally, a robustness analysis is carried out based on a train-test methodology, which analyzes the required number of train data needed to fit the model, avoiding overfitting.

2. Methodology

The methodology followed to obtain compact prediction models starts with studying a high-fidelity experimental data set obtained from

a variable-speed compressor, which will be used as a reference. For this step, it is essential to use real empirical data obtained from a laboratory test bench rather than catalog data, as the latter tends to be predicted from pre-fitted models instead.

The data used for this study has been obtained from a compressor test bench whose complete description is available in [6]. On this test bench, a variable-speed scroll compressor working with R290 was tested over an extensive envelope of condensing and evaporating temperatures (Fig. 1). This same pattern was repeated at different speeds ranging from 30 to 110 Hz to study the influence of speed on performance. It has to be noted that the test matrix was designed to be as orthogonal as possible to make it possible to study how each variable affects the performance independently. In total, 133 different conditions were tested, and each individual result can be accessed at [6].

From the study of the empirical data, the main trends are retrieved, which are then employed to design and improve predicting correlations for mass flow, consumption and discharge temperature, focusing on the dependence of these variables with speed.

Then, to ensure that the conclusions obtained for this compressor technology can be generalized for multiple compressor models and technologies, the obtained correlations will be validated against the experimental datasets summarized in Table 1.

In Table 1, the first three columns represent experimental data obtained by the authors in the mentioned compressor test bench [6]; the two first datasets were already reported in a previous study [6] and the third data set is reported as complementary material in this manuscript. The other datasets (columns 4 to 7) represent datasets of variable-speed compressors published in other studies.

Cuevas and Lebrun [13] provided a dataset with 48 different conditions at five different speeds. Even if it does not cover the complete compressor envelope, the test matrix maps a significant portion of it and presents quite an orthogonal design. Additionally, the experimental uncertainty was low.

Shao et al. [14] tested a rotary compressor working with R22. However, in his study, only the experimental ratio of mass flow and consumption for nominal speed seems to be provided, not the absolute results (as for nominal speed only a 6-coefficient correlation is presented). Consequently, this dataset is partially filtered by the model used and not exclusively empirical. Nevertheless, it was considered in this study, so a direct comparison can be made between their correlation and other alternatives.

Winandy et al. [12] published an experimental data set of a mechanically-driven open-type reciprocating compressor working with R12. The piston had a significant displacement and the tested speeds were very low, which is unusual for domestic heat pumps. The dataset consists of only 25 conditions tested at three different speeds ranging from 6 to 11 Hz. Both power and mass flow measurements were indirect, with a high stated uncertainty of 5 and 3 %, respectively.

Finally, Moradi et al. [15] studied the performance map of a heat pump and published a performance data set with 44 test results over five different speeds. The test matrix was not centered on the compressor envelope but on the HP instead. Consequently, higher pressure ratios are tested as compressor speed increases, so studying the speed effect *ceteris paribus* is challenging. Additionally, the mass flow measurement was indirect and the power meter resolution was 100 W, resulting in a high observed experimental uncertainty.

All the mentioned variable-speed compressors were tested at constant superheat conditions and consequently, the effect of suction conditions on performance cannot be studied. That is why the effect of suction conditions will be studied in another section using the dataset AHRI21 [16] for a fixed-speed compressor and the conclusions are expected to be extrapolated for variable-speed compressors.

In the AHRI21[16] dataset, five different refrigerants were tested in the same compressor, and for each refrigerant, three complete experimental maps were obtained for different suction conditions; one for SH = 11 K, other at SH = 22 K and the last keeping the suction temperature at 18 °C. A summary of the complete dataset is displayed in Table 2.

For the evaluation of the accuracy (goodness of fit) of the proposed models, RMSE and CV estimators will be used. Root Mean Squared Error (RMSE) represents the standard deviation of the prediction errors and it is reported with the same units of the modeled variable. Coefficient of Variation of RMSE (CV) constitutes a normalized RMSE and could be used as an estimator of the expected relative error. It can be used to compare models when applied to different ranges.

$$CV = \frac{RMSE}{\bar{X}} = \frac{1}{\bar{X}}\sqrt{\frac{\sum_{n=1}^{N}(\hat{y}_t - y_t)^2}{N}} \tag{3}$$

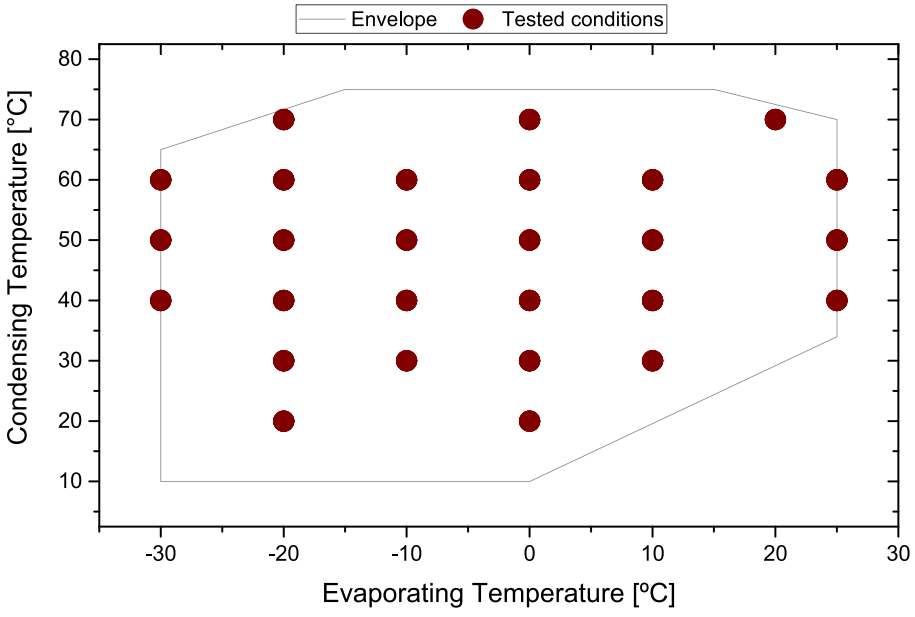

Fig. 1. Test matrix and compressor envelope.

Table 1
Summary of variable-speed compressor datasets.

	Scroll-R290	Scroll-R410A	Scroll-R454C	SCROLL-R134a	Rotary-R22	Piston-R12	Piston-R134a
Source	Exp. [6]	Exp. [6]	Exp.	Cuevas[13]	Shao[14]	Winandy[12]	Moradi[15]
Tech	scroll	scroll	scroll	scroll	rotary	piston	piston
Displ [cm^3]	46	44.5	44.5	54.25	20.7	680	74.83
Refr	R290	R410A	R454C	R134a	R22	R12	R134a
Te [°C]	−30 / 25	−30 / 7	−15/44	14 / 68	−10 / 15	−26 / 23	−13 / 2
Tc [°C]	20 / 70	25 / 49	28 / 85	39 / 101	40 / 60	8–68	19 / 65
fc [Hz]	30 / 110	15 / 100	15 / 100	35 / 75	30 / 120	6–11	30 / 50
fc_nom [Hz]	70	60	60	50	60	6	45
SH [K]	10	10	10	7	11	28	12
Tests	133	35	87	48	296	25	44

Table 2
Summary of multiple SH dataset.

	SH11	SH22	T1_18
Compressor Model	ZS21KAE-PFV		
Technology	Hermetic scroll		
Displacement [cm^3]	50.96		
Refrigerants	R404A, ARM31a, D2Y65, L40, R32_R134a		
Tevap Range [°C]	−23 / 1.6		
Tcond Range [°C]	21 / 60		
Nominal Speed [Hz]	60		
Suction Conditions	SH = 11 K	SH = 22 K	T1 = 18 °C
Tests	63	63	63

3. Results

3.1. Mass flow

3.1.1. Experimental results

In this section the obtained mass flow results of the intensively tested scroll-290 compressor are analyzed.

In Fig. 2 the mass flow evolution is displayed either based on temperatures and pressures.

The variables that affect mass flow the most are compressor speed and the evaporation condition. It should be noted that the influence of condensing temperature is very subtle and the variation of mass flow with it is barely perceptible with the scale of the graph. It is also worth mentioning that the response surface is almost linear if mass flow is plotted against the evaporating pressure.

In Fig. 3, the experimental volumetric efficiency – defined with Eq.(4) – is plotted against pressure ratio (PR), and the different lines represent the different tested speeds.

$$\eta_v = \frac{\dot{m}}{\rho_1 f_c displ} \tag{4}$$

Volumetric efficiency is close to 1 at low PR and decreases quite linearly as PR increases. Volumetric efficiency does not show a strong dependency on speed at medium and high speeds. However, volumetric efficiency clearly decreases at low speeds, and this decrease is more significant as PR increases.

This reduction in volumetric efficiency can be explained by internal leakages in the compressor chamber. As compression speed decreases, the compression is slower and refrigerant has more time to leak. Additionally, in the tested compressor, the oil sump is in the bottom part of the compressor, and a borehole in the shaft (acting as a centrifugal pump) is responsible for pumping the oil from the carter to the compressor chamber and the main bearings. The centrifugal action is significantly reduced at low speeds, and the pumped oil can be insufficient to create a hydrodynamic film to correctly seal the compression chamber, increasing the leakages and dropping the volumetric efficiency.

3.1.2. Model

As introduced in the first section, historically mass flow has been modeled with correlation based on working temperatures (T_e and T_c). However, as deduced from Fig. 2, the fact of using pressures instead of temperatures as modeling variables could significantly reduce the required model complexity. The AHRI-540 standard [1] uses 10 coefficients for fixed-speed compressors, including up to cubic terms, but if pressures are used as modeling variables, an acceptable accuracy could be obtained using fewer coefficients. In this line Marchante-Avellaneda et al. [17] proposed a model based on working pressures and using only four coefficients for fixed-speed compressors Eq.(5).

$$\dot{m} = k_0 + k_1 P_e + k_2 P_c + k_3 P_e P_c \tag{5}$$

In order to model the effect of speed in mass flow, Shao et al. [14] proposed an approach using a 3-coefficient quadratic equation to model the ratio between mass flows at any speed and the nominal one (k_m) [Eq. (2)] and proved that these ratios were dependent only on speed not on working conditions. This methodology allows to model the compressor in a decoupled manner: with one equation representing how mass flow evolves at one speed (typically the rated one) and another to model the mass flow variation with speed.

However, the ratio k_m is heavily dependent on speed differences and it is known a priory that doubling speed will approximately double the mass flow. Consequently, modeling k_m as a function of speed differences ends up adjusting this pre-known behavior resulting in a linear term very close to unity, an intercept very close to zero and a quadratic term with low significance.

In this study, to solve that limitation, the ratios of volumetric efficiencies (k_v) will be used instead to model the speed influence on the performance. The process of deducing k_v from k_m is represented in Eq.(6) and concludes that the relation between one and the other is just the speed ratio between any speed and the nominal one ($f_{c,rat}$).

$$k_m = \frac{\dot{m}}{\dot{m}_{nom}} = \frac{f_c}{f_{c,nom}} \frac{\eta_v}{\eta_{v_{nom}}} \frac{\cancel{displ\ \rho_1}}{\cancel{displ\ \rho_1}} = f_{c,rat}\ k_v \tag{6}$$

In Fig. 4, the k_m and k_v evolution with speed is displayed for two different compressors; Shao's compressor in the first column and the reference compressor in the second column.

In the first row the quadratic fit of k_m is represented with a dashed red line, it should be noted that it is practically indistinguishable from a straight line of slope 1. However, if k_v are represented, the quadratic evolution becomes clear and the decrease of volumetric efficiency at low

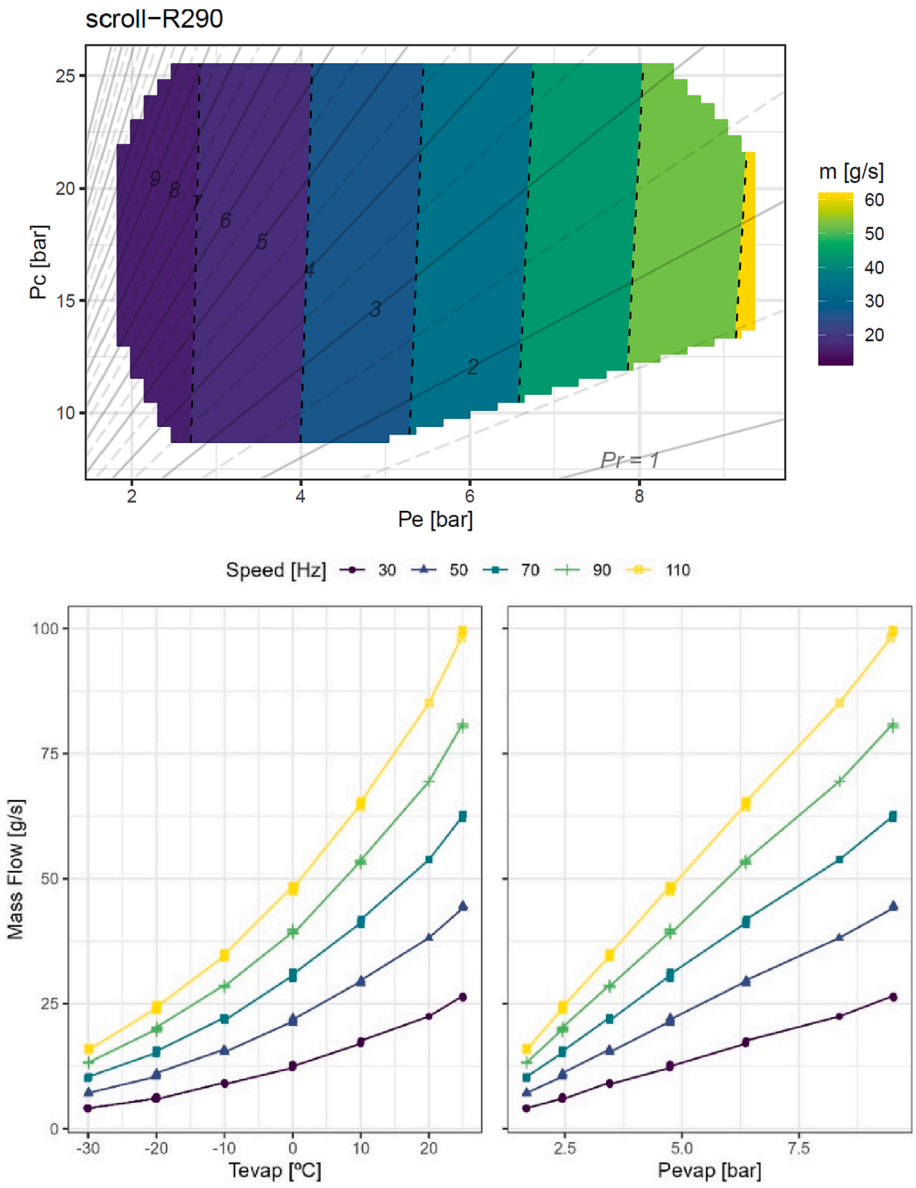

Fig. 2. Evolution of mass flow with compression conditions at nominal speed (Up). Evolution of mass flow as a function of evaporating temperatures (Down-left) and pressures (Down-right).

speeds becomes evident. Fig. 4 also shows that the variation range of k_v is very narrow compared with k_m and typically values close to one are achieved meaning that the effect of speed on η_v is reduced and consequently a simplified model as Eq.(7) could be used.

$$\dot{m} = \dot{m}_{nom}\, k_m = \dot{m}_{nom}\, f_{c,rat}\, \cancel{k_v} = (k_0 + k_1 P_e + k_2 P_c + k_3 P_e P_c)\, f_{c,rat} \tag{7}$$

Additionally, from Fig. 4 it is observed that k_v reaches a maximum at a given speed and the overall behavior is parabolic. Accordingly, if extra accuracy is needed and the effect of speed in volumetric efficiency needs to be acquainted the proposed correlation in Eq.(6) was proposed.

$$k_v = k_m \frac{1}{f_{c,rat}} = \frac{\dot{m}}{\dot{m}_{nom}} \frac{f_{c,nom}}{f_c} \sim k_4 \left(f_{c,rat} - \frac{k_5}{f_{c,nom}} \right)^2 + k_6 \tag{8}$$

By definition, k_v must be 1 at nominal speed and thus, that constraint can be used to define b_3 as a function of the other two fitting coefficients [Eq.(9)], resulting in a correction expression with only two coefficients instead of three as the one proposed by Shao et al.

$$k_6 = 1 - k_4 \left(1 - \frac{k_5}{f_{c,nom}} \right)^2 \tag{9}$$

Furthermore, due to the formulation of the correlation, both fitting coefficients represent important information: k_5 represents the speed at which the volumetric efficiency reaches its maximum and k_4 represents the curvature of the parabola, in other words the influence of speed on η_v.

Finally, if equations Eq.(7) and Eq.(8) are combined, a general expression is obtained to predict mass flow at any given condition of working pressures and speed [Eq.(10)].

$$\begin{aligned} \dot{m} &= \dot{m}_{nom} f_{c,rat} k_v \\ &= (k_0 + k_1 P_e + k_2 P_c + k_3 P_e P_c)\, f_{c,rat} \left[k_4 \left(f_{c,rat} - \frac{k_5}{f_{c,nom}} \right)^2 + k_6 \right] \end{aligned} \tag{10}$$

It is important to note that the general equation has only 6 coefficients as b_3 is calculated with Eq.(9).

Fig. 5 represents the correlation graph of the presented model

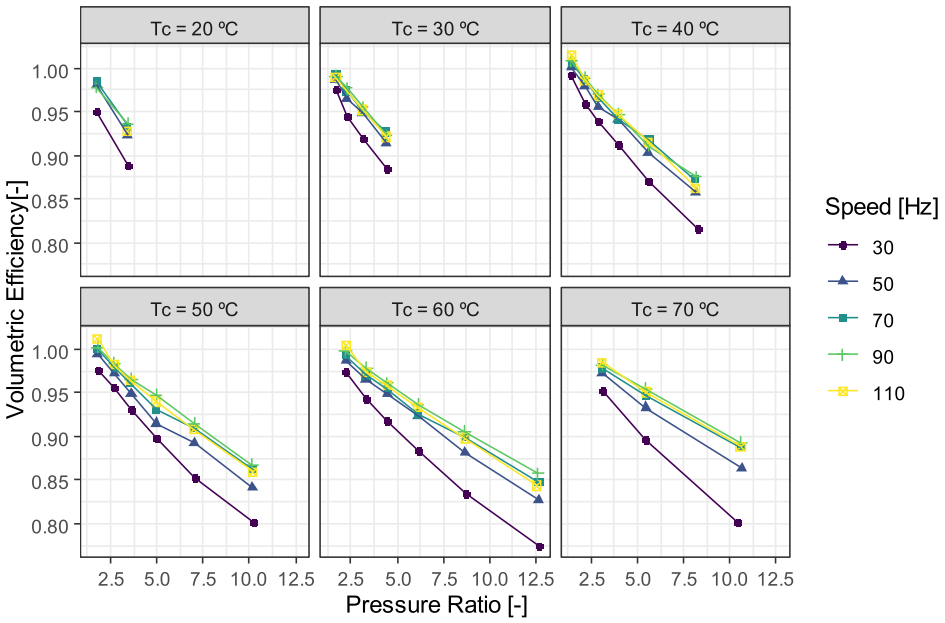

Fig. 3. Evolution of volumetric efficiency with pressure ratio and speed.

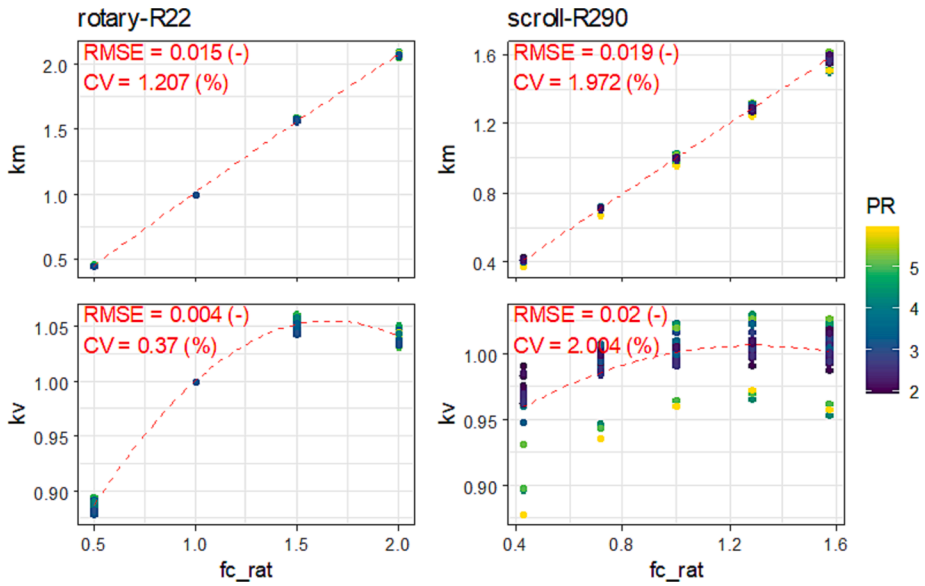

Fig. 4. k_m and k_v evolution with speed for two different compressors.

applied to "scroll-R290" compressor. The resulting modeling error is low, with a RMSE of 0.219 g/s and a CV lower than 1 %.

To validate the obtained result, the model was also tested against the other experimental datasets described in Table 1 and the obtained RMSE and CV are displayed in Fig. 6.

In Fig. 6 the baseline is reported by the AHRI-20 model which, when fitted with all the experimental data set, provides the highest accuracy as it has many fitting coefficients (20 coefficients in total). It should be remembered though, that the number of coefficients in AHRI-20 model was not justified and having a high number of coefficients will always adjust better the train data but risks overfitting; incurring in higher prediction errors with unseen data as seen in Section 3.2.

Additionally, to AHRI-20 results, the modeling errors of Shao correlation and the new proposed model are also displayed. It is remarkable how, with less than half the number of fitting coefficients, both obtain similar fitting results compared to AHRI-20 in most compressors. This is other indicator that using 20 coefficients is overmuch.

Comparing Shao and the proposed correlation, the proposed correlation performs better consistently, even with less fitting coefficients (six versus nine). The only data set that Shao had better accuracy is piston-R12 in which the difference in accuracy falls in the experimental uncertainty band.

In the piston-R12 compressor, the difference between the modeling accuracy of AHRI 20 and the compact models increases which can be explained by the high experimental error and the low number of tests. AHRI-20 has 20 fitting coefficients and the dataset only 25; consequently, the chances are high that AHRI-20 is overfitting the given dataset.

Finally, in piston-R134a the obtained CV surpass the 5 % threshold even for AHRI-20 model which clearly indicates a high experimental error. However, what is remarkable is the impossibility of Shao's model to adjust the data. This fact can be explained as the tested temperature range was not the same for all tested speed and thus important extrapolations are involved.

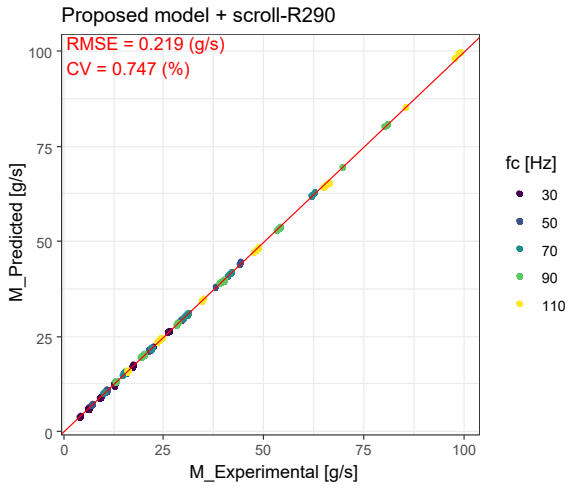

Fig. 5. Correlation plot of mass flow model applied to reference compressor.

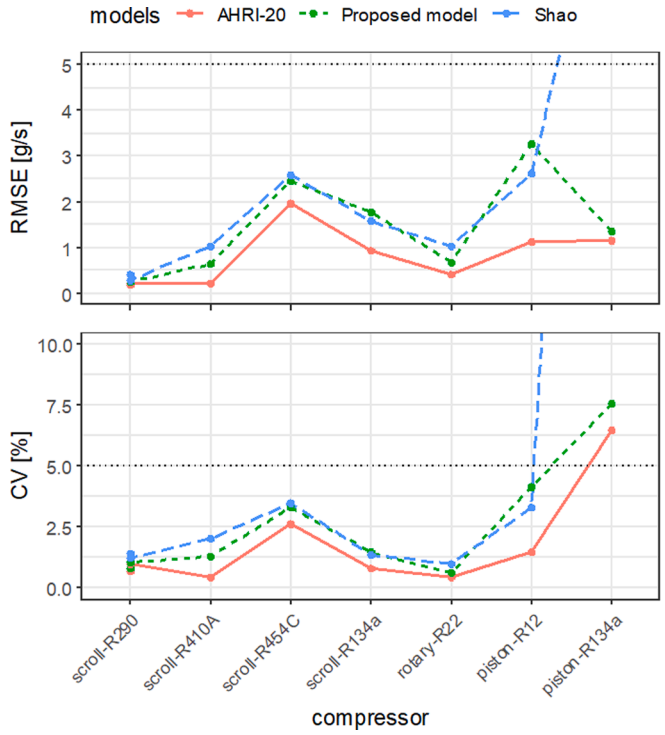

Fig. 6. Goodness of fit of mass flow models applied to different data sets.

Proven the accuracy of the proposed model, the obtained fitted coefficients for the different compressors are listed in Table 3 (using g/s, bar and Hz) together with its fitting accuracy expressed as RMSE, MRE and CV. Note that the coefficient *k5* represents the speed at which the volumetric efficiency becomes maximum and, in the studied compressors, it tends to be in the high-speed domain of each compressor.

3.2. Energy consumption

3.2.1. Experimental results

This section analyses the energy consumption results of the intensively tested scroll-290 compressor.

In Fig. 7 the evolution of energy consumption with working temperatures and speed is displayed.

The main variable affecting consumption is the compressor speed, which affects the energy consumption proportionally. For a given speed, the variable affecting the most the energy consumption for the analyzed compressor is the condensing temperature. Regarding the evaporating temperature, when it increases two counteracting phenomena occur: firstly, the suction pressure and density increase, increasing the mass flow and thus increasing the expected energy consumption; secondly, the pressure ratio reduces thus decreasing the expected consumption. These counteracting phenomena make the energy consumption practically independent on suction temperatures for pressure ratios higher than three for the selected compressor working at nominal speed. This analysis was conducted with an scroll compressor and it could be different for piston as stated in [18].

Fig. 8 shows the evolution of compressor efficiency (defined with Eq. (11)) with pressure ratio and speed – at different condensing temperatures –.

$$\eta_c = \frac{\dot{m}(h_{2s} - h_1)}{\dot{W}_c} \tag{11}$$

It should be pointed out that compressor efficiencies at central speeds (50, 70 and 90 Hz) behave homogeneously, having a maximum between pressure ratios of 2.5 and 3. This maximum is explained by the scroll's built-in volume ratio; for lower *PRs* the refrigerant is discharged with an overpressure that is dissipated in the discharge valve (explaining the rapid decrease in efficiency). The designed scroll's built-in volume ratio is parameter that is not displayed in catalogs and thus it is not known a priori; however similar results have been reported by Winandy et al [19].

At low speeds and high condensing temperatures, a decrease in compressor efficiency is manifested. Cuevas and Lebrun [13] suggested a possible explanation of this effect: a lack of lubrication at low compressor speeds, which increased internal leakages and possibly also frictional losses. The internal leakages are related to the pressure difference, which explains why these become more relevant at high condensing temperatures.

Additionally, the compressor efficiency decreased also slightly at high speeds due to increased mechanical losses. These mechanical losses do not depend heavily on the working temperatures; thus, at lower condensing temperatures where the compressor has a lower consumption, they have a major impact on efficiency.

Another variable that can be analyzed is the specific consumption, defined as the ratio between energy consumption and refrigerant mass flow [Eq.(12)]. Its evolution with compression conditions is displayed in Fig. 9.

$$\dot{W}_{esp} = \dot{W}_c / \dot{m} \tag{12}$$

The evolution of the specific energy consumption seems to have a correlation with the pressure ratio as the isolines tend to be quite parallel to the pressure ratio lines. However, the isolines tend to converge at a virtual point lower than the convergence point of pressure ratio lines [18].

On the other hand, specific consumption seems to be independent with speed except for the lowest speed in which an increase of specific consumption is evident and it becomes more significant at higher pressure ratios. The increase in specific consumption at low speeds is explained by a decrease of volumetric and compressor efficiency due to lubrication problems and could be used to limit the compressor envelope.

3.2.2. Model

As observed in the obtained results, the specific consumption is the simplest variable to model due to its smooth and linear behavior. The modeling of power consumption through a correlation based on specific consumption was already proposed for fixed-speed compressors by Marchante-Avellaneda et al. [18], whose general expression is displayed in Eq.(13). In his study, Marchante-Avellaneda et al. [18] also concluded that this correlation could apply to both reciprocating and scroll

Table 3
Model coefficients and goodness of fit of the mass flow model applied to the different compressors.

	scroll-R290	scroll-R410A	scroll-R454C	scroll-R134a	rotary-R22	piston-R12	piston-R134a
k0	−0.810***	−2.910	−5.716**	3.873	−7.894***	−12.569*	1.130
k1	6.815***	10.290***	12.281***	12.441***	20.278***	26.817***	8.789**
k2	−0.019*	−0.215**	−0.121	−0.681***	−0.298***	−0.241	0.466
k3	−0.008***	−0.008	−0.059***	0.021+	−0.128***	−0.269+	−0.300
k4	−0.026***	−0.073***	−0.088**	−0.198***	−0.125***	0.143	−0.050
k5	104.386***	92.450***	72.354***	55.535***	99.723***	7.850***	79.378
Num.Obs.	133	35	87	48	296	25	44
RMSE	0.22	0.64	2.46	1.76	0.66	3.25	1.34
CV	0.75	1.23	3.28	1.47	0.60	4.12	7.54

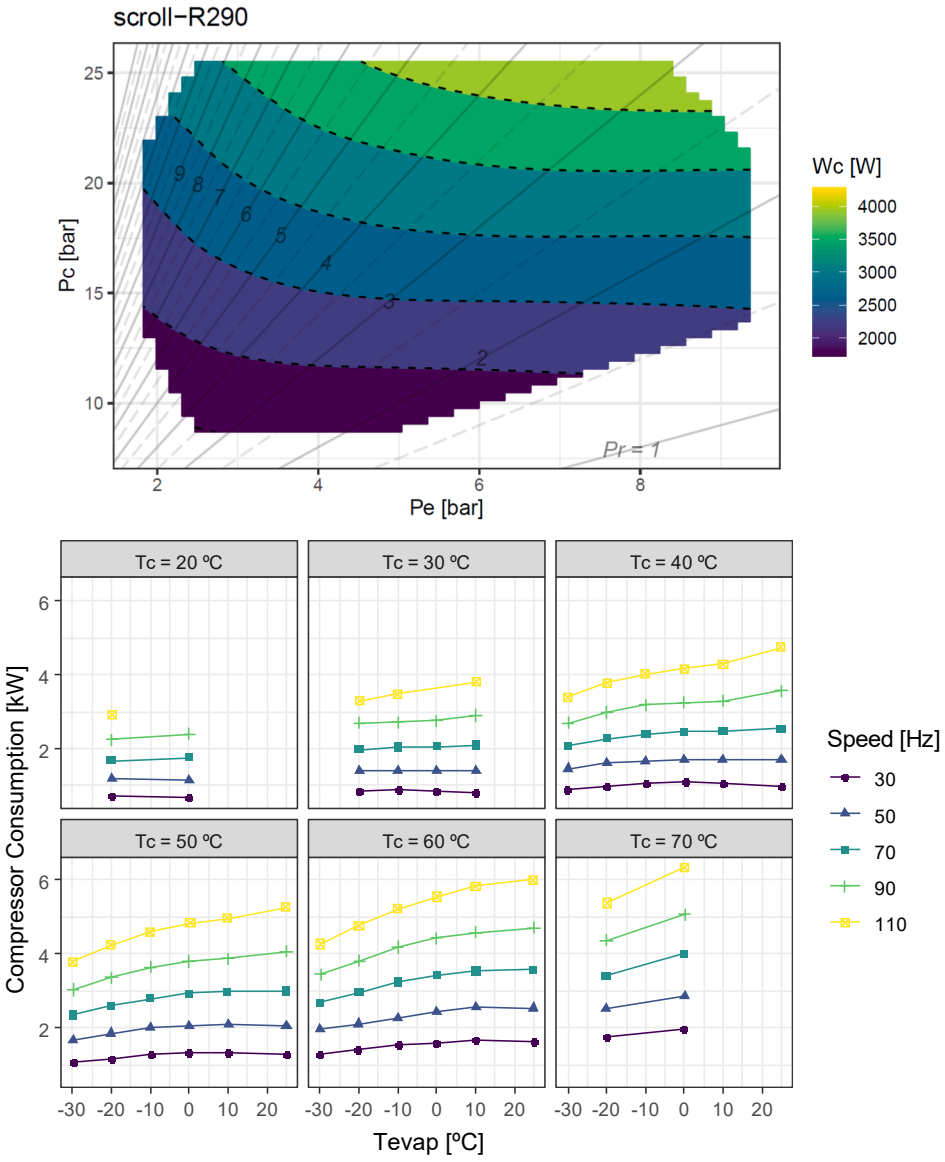

Fig. 7. Evolution of energy consumption with compression conditions at nominal speed (Up). Evolution of energy consumption as a function of evaporating temperatures and speed (Down).

compressors as they behave homogeneously in the domain of specific consumption.

$$\dot{W}_{esp} = \dot{W}_c / \dot{m}_{pred} = k_0 + k_1 P_r^{'} + k_2 P_r^{'2} + \cdots + k_n P_r^{'n}$$

$$with\ P_r^{'} = \frac{P_c - z_c}{P_e - z_e} \tag{13}$$

Being $k_{\#}$, z_c and z_e the fitting parameters and the determination of the order (n) of the correlation is done iteratively. The required order of Eq. (13) for the studied dataset was one, as adding a quadratic term did not significantly improve the model accuracy. Regarding z_c and z_e they represent a translation of the cartesian origin to the convergence point of the *iso*-specific-consumption lines in Fig. 9-LEFT as stated in [18].

It should be noted that the specific energy consumption correlation is coupled with the mass flow model. Consequently, the uncertainty of

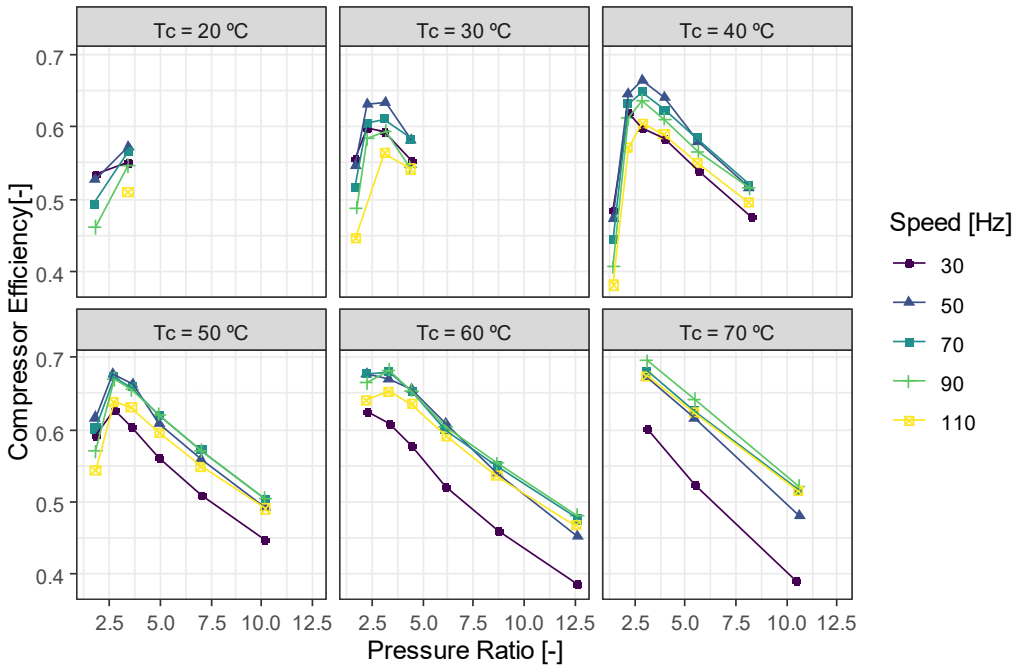

Fig. 8. Evolution of compressor efficiency.

mass flow measurements will affect the accuracy of the energy consumption model. That is why using predicted values obtained from a pre-fitted mass flow model is generally preferred over empirical results, as using a correlation partially filters the noise level introduced by experimental uncertainty.

This correlation also has the advantage of partially accounting for the speed effect (as it normalizes the consumption with the mass flow) and thus, it can be used to extrapolate energy consumption to different speeds, especially if the compressor efficiency is not greatly affected, which typically happens at speeds close to rated speed.

If higher precision is required in the analysis of the speed effect, an approach similar to the one followed by Shao et al. [14] can be followed. Shao et al. [14] defined a power ratio with respect to rated speed (k_p) and modeled it with a 3 coefficients quadratic equation [Eq.(1)]. However, as happened with mass flow, it ends up modeling a pre-known behavior as consumption is expected to approximately double when speed is doubled.

To correct that, the ratio k_c will be studied instead of k_p. k_c is defined in Eq.(14) as the ratio of specific consumptions. It should be noted, that this ratio also represents the inverse of the ratio of compressor efficiency and can be deduced from k_p and k_m rations [Eq.(15)].

$$k_c = \frac{\dot{W}_{esp}}{\dot{W}_{esp,nom}} = \frac{\frac{\dot{W}_c}{\dot{m}_{pred}}}{\frac{\dot{W}_{c,nom}}{\dot{m}_{pred,nom}}} = \frac{\frac{\dot{m}_{pred,nom}\cancel{\Delta h_{is}}}{\dot{W}_{c_{nom}}}}{\frac{\dot{m}^{\#}\cancel{\Delta h_{is}}}{\dot{W}_c}} = \frac{\eta_{c,nom}}{\eta_c} \tag{14}$$

$$k_c = \frac{\frac{\dot{W}_c}{\dot{m}_{pred}}}{\frac{\dot{W}_{c,nom}}{\dot{m}_{pred,nom}}} = \frac{k_p}{k_m} \tag{15}$$

Fig. 10 shows a comparison between the evolution of k_p and the inverse of k_c with speed for two different compressors (Shao's compressor in the first column and the reference compressor in the second column). The inverse of k_c was plotted (instead of k_c) as it represents the compressor

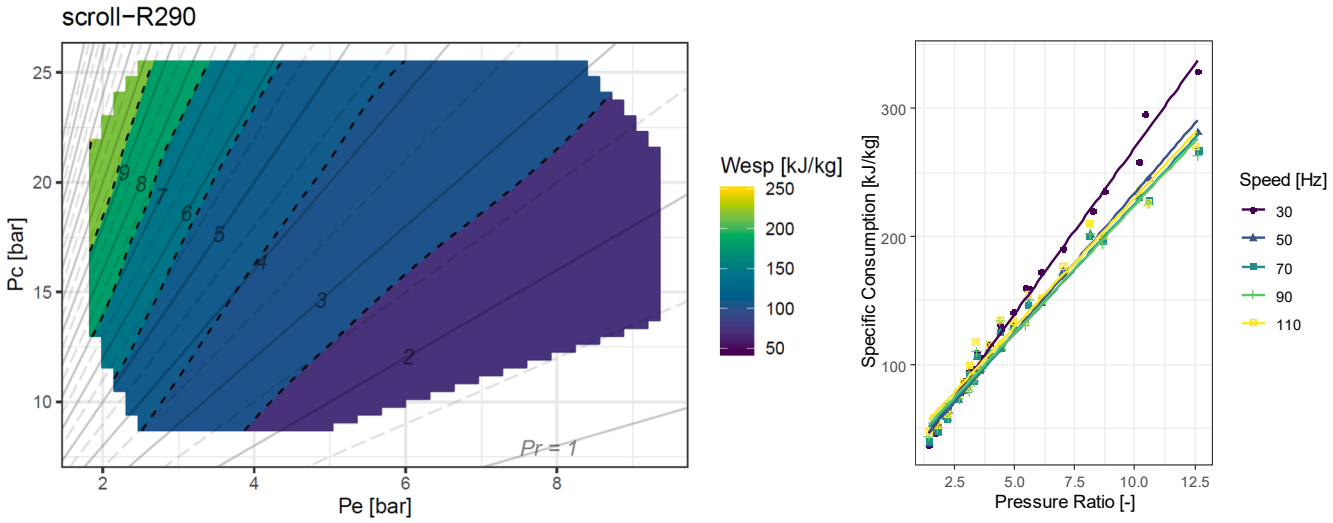

Fig. 9. Specific consumption evolution with operating pressures (LEFT). Evolution of specific consumption with pressure ratio and speed (RIGHT).

efficiency ratio, and its maximum represents the most efficient condition.

The evolution of k_p with speed ratio is plotted in the first row. The evolution presents a slight curvature but it is not far from a straight line with 45° slope which implies that k_p has a strong dependence with speed ratio. This linear dependence is normalized in the case of k_c which allows to retrieve more significant results from its study. In particular, it permits to analyze how speed affects compressor efficiency. In both compressors the optimum compressor efficiency is obtained at speeds close to the nominal and in the rotary-R22 data set the effect of speed in compressor efficiency is much more significant reaching a decrease in efficiency close to 25 % at low and high speeds.

To model the evolution of k_c with compressor speed, the same parabola equation used to model k_v in Eq.(8) is proposed.

$$k_c = \frac{\dot{W}_{esp}}{\dot{W}_{esp,nom}} = \frac{\eta_{c,nom}}{\eta_c} \sim k_4 \left(f_{c,rat} - \frac{k_5}{f_{c,nom}} \right)^2 + k_6$$

$$\text{with } k_6 = 1 - k_4 \left(1 - \frac{k_5}{f_{c,nom}} \right)^2 \tag{16}$$

With this formulation k_5 represents the speed at which compressor efficiency reaches its maximum and k_4 represents the influence of speed on k_c.

If both Eq.(13) and Eq.(16) are combined, a general expression for the energy consumption of variable-speed compressors can be written as Eq.(17).

$$\dot{W}_c / \dot{m}_{pred} = \left(k_0 + k_1 \frac{P_c - k_2}{P_e - k_3} \right) \left[k_4 \left(f_{c,rat} - \frac{k_5}{f_{c,nom}} \right)^2 + k_6 \right] \tag{17}$$

Resulting in a correlation with six coefficients which, compared to Shao et al. [14] model with nine, implies a reduction of three coefficients. The result of training the proposed correlation with the complete data set of the reference compressor is displayed in Fig. 11.

The obtained RMSE is lower than 100 W and the CV is close to 3 % for the reference compressor. In order to validate that result, the energy consumption model in Eq.(17) was fitted for all the presented data sets in Table 1 and the model accuracy is plotted in Fig. 12 among the fitting results obtained by Shao et al. [14] model and using as baseline the goodness of fit of AHRI-20 model.

Both compact models have similar modeling errors and tend to achieve less than 5 % CV values. Despite having more coefficients (9 vs 6), only two data sets were adjusted better by Shao et al. [14] model and with very subtle differences. Additionally, it should be noted the case of the rotary-R22 compressor, which was reported in Shao et al. [14], and how the proposed model managed to perfectly fit the dependence of compressor efficiency with the speed, performing significantly better than Shao et al. [14] model itself and obtaining very similar results compared with AHRI-20 model (but using less than one-third of coefficients). However, even if the proposed model fitted very accurately, it should be remembered that the rotary-R22 data set was partially reconstructed using pre-fitted models and more experimental data from rotary compressors would be needed to generalize the results to all rotary compressors.

AHRI-20 model managed to fit all datasets with reduced prediction errors, but it should be noted that the coefficient fit was made using the complete data set and, when this happens, models having a great amount of coefficients tend to perform better but risk overfitting when adjusted with limited train data. The overfitting in AHRI-20 model was evaluated in Section 3.2 Robustness Analysis.

In Table 4 the fitted coefficients of the proposed model are displayed for the different compressor data sets (using kJ/kg, bar and Hz as units). k_1 tends to be the most significant parameter as it models the variation of specific consumption with the corrected pressure ratio. It should also be noted that k_1 and k_2 represent z_c and z_e respectively which represent how the point of convergence of specific consumption isolines are displaced from the origin in Fig. 9-LEFT. The displacement tends to be more relevant in the condensing pressure axes and negative (which was expected to account for no-load losses). Finally, k_5 represents the speed at which the compressor runs more efficiently; the obtained optimum speeds tend to be slightly lower than the ones obtained for volumetric efficiency which indicates that the compressor efficiency drop at very high speeds is lower than the drop seen in volumetric efficiency.

3.3. Discharge temperatures

3.3.1. Experimental results

The variable-speed scroll compressor working with R290 was tested with a suction temperature 10 K higher than the evaporating temperature and at a controlled ambient temperature of 35 °C. In Fig. 13, the

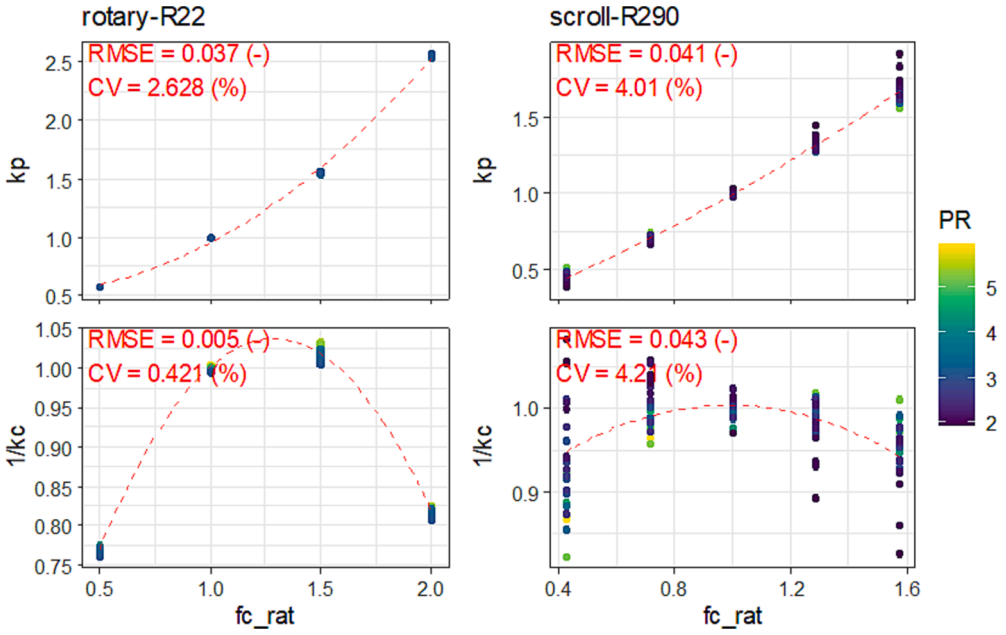

Fig. 10. k_p and k_c evolution with speed for two different compressors.

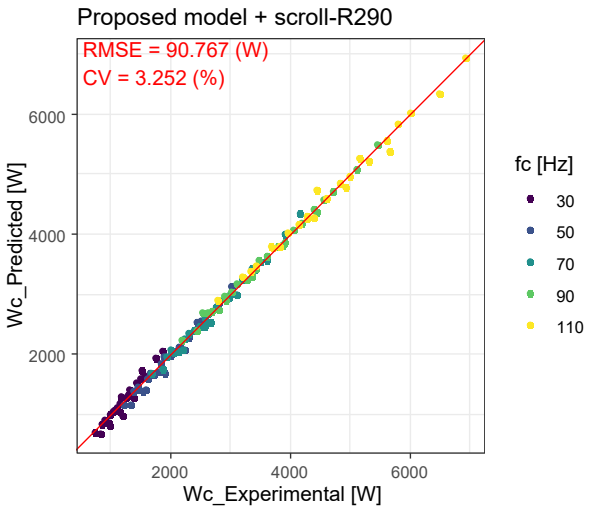

Fig. 11. Correlation plot of energy consumption model applied to reference compressor.

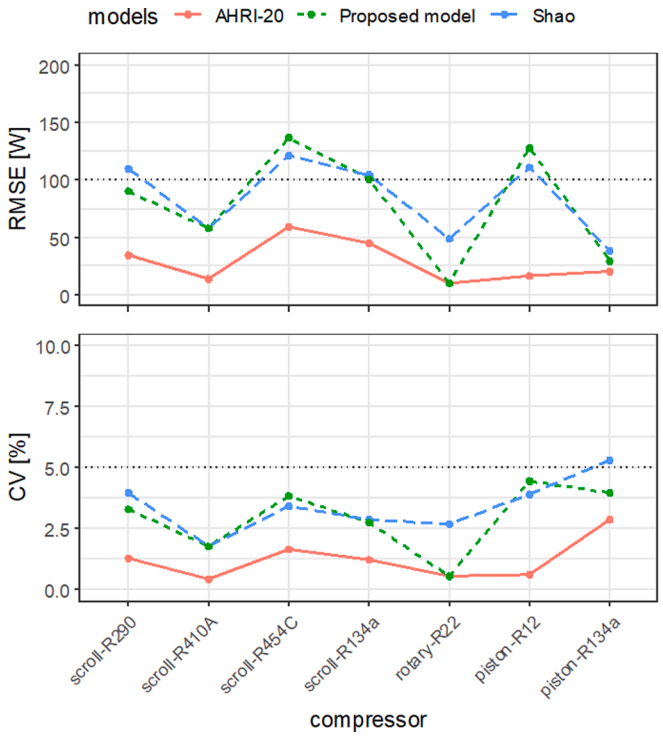

Fig. 12. Goodness of fit of energy consumption models applied to different data sets.

experimental discharge temperatures are plotted. The left graph displays the evolution of discharge temperatures around the envelope at rated speed. And in the graph at the right, all the tested results are displayed as a function of pressure ratio, compressor speed and condensing temperatures.

Fig. 13 – LEFT shows that the highest obtained discharge temperatures are produced in the high-pressure ratio region; in fact, the working envelope is typically limited in the high pressure region by the maximum allowable discharge temperature, as most frequently used lubricating oils degrade at temperatures around 120–130 °C.

In Fig. 13 – RIGHT, discharge temperature shows a high dependence on pressure ratio and condensing temperature. However, the effect of compressor speed in discharge temperatures is small and typical variations lower than 5 K are obtained from minimum to maximum speed.

Typically, modeling discharge temperatures directly is not recommended as the obtained predictions are only valid for the defined SH. That is why, modeling other variables less dependent on the suction conditions is typically preferred. Fig. 14 plots the compressor isentropic efficiencies defined in Eq.(14).

$$\eta_{is} = \frac{h_{2s} - h_1}{h_2 - h_1} \tag{18}$$

It can be noted that the evolution of isentropic efficiency is very similar to the observed evolution of the compressor efficiency, with a maximum at the built-in pressure ratio. This variable is still significantly dependent on compression conditions and complex models would be needed to model their behavior accurately.

Another dimensionless variable that could be studied is the electro-mechanical efficiency. It is defined as the ratio between the energy transferred to the refrigerant and the energy consumption [Eq.(19)] and its evolution with the compression conditions is displayed in Fig. 15.

$$\eta_{e-m} = \frac{\eta_c}{\eta_{is}} = \frac{\dot{m}(h_2 - h_1)}{\dot{W}_c} \tag{19}$$

Electro-mechanical efficiency shows low dependence with compression conditions for medium and high speeds with stable values between 0.85 and 0.9. However, as speed decreases, a strong dependence with pressure ratio appears and the efficiency drops as pressure ratio increases.

3.3.2. Model

In the literature, the most extended approach to model discharge temperatures is to assume a constant isentropic efficiency or to model power losses as two terms: a term depending on total compression work and a constant term. This last methodology is the one proposed by ASHRAE in Toolkit [11], and its formulation is displayed in Eq.(20) where the two fitting parameters are: the constant power losses (W_{loss_0}) and the fraction of usefull energy that is lost as heat (α).

$$\dot{W}_c = \dot{m}(h_2 - h_1)(1 + \alpha) + W_{loss_0} \tag{20}$$

Eq.(20) can also be rewritten as a function of the previously introduced electro-mechanical efficiency, resulting in Eq.(21).

$$\eta_{em} = \frac{\dot{m}(h_2 - h_1)}{\dot{W}_c} = \frac{1}{1 + \alpha}\left(1 - \frac{W_{loss_0}}{\dot{W}_c}\right) = k_0 - \frac{k_1}{\dot{W}_c} \tag{21}$$

However, this expression does not consider the pressure ratio or the compressor speed, which were proven to affect electro-mechanical losses in variable-speed compressors (Fig. 15). Consequently, if extra accuracy is needed, additional terms can be added, resulting in the model of Eq.(22). The predicted electro-mechanical efficiencies with this latter model are displayed in Fig. 15 as solid lines.

$$\eta_{em} = k_0 + k_1 PR + k_2 \frac{PR}{f_{c,rat}} + k_3 \frac{1}{\dot{W}_c} \tag{22}$$

Eq.(22) was the result of the analysis of the specific power losses and their dependence with the studied variables. For more information, please refer to Appendix 1: Electro-mechanical losses.

Once electro-mechanical losses are modeled, the predicted discharge enthalpy can be calculated using Eq.(19). And finally, knowing discharge enthalpy and pressure, the predicted discharge temperature can be computed using any thermodynamic database [20].

If the proposed model in Eq.(22) is fitted with the reference compressor, the correlation graph in Fig. 16 is obtained with a RMSE lower than 1 K for discharge temperatures.

To validate the presented model, it was fitted to the other

Table 4
Model coefficients and goodness of fit of the energy consumption model applied to the different compressor data sets.

	scroll-R290	scroll-R410A	scroll-R454C	scroll-R134a	rotary-R22	piston-R12	piston-R134a
k0	−0.251	−2.783+	−11.618***	−5.468***	−0.662***	0.665	2.345
k1	21.030***	14.283***	18.378***	12.970***	4.315***	9.862***	11.775*
k2	−6.696***	−2.328*	−1.921*	−0.029	−1.487***	−2.578*	−1.974
k3	−0.511***	0.214	−0.539**	0.629**	−0.092**	−0.398	−1.000
k4	0.185***	0.139***	0.144***	0.545***	0.533***	−0.165	0.293
k5	72.916***	65.960***	64.293***	58.650***	77.625***	11.013***	37.577***
Num.Obs.	133	35	87	48	296	25	43
RMSE	90.77	57.73	137.15	99.88	9.89	127.34	30.32
CV	3.25	1.75	3.84	2.72	0.54	4.46	4.13

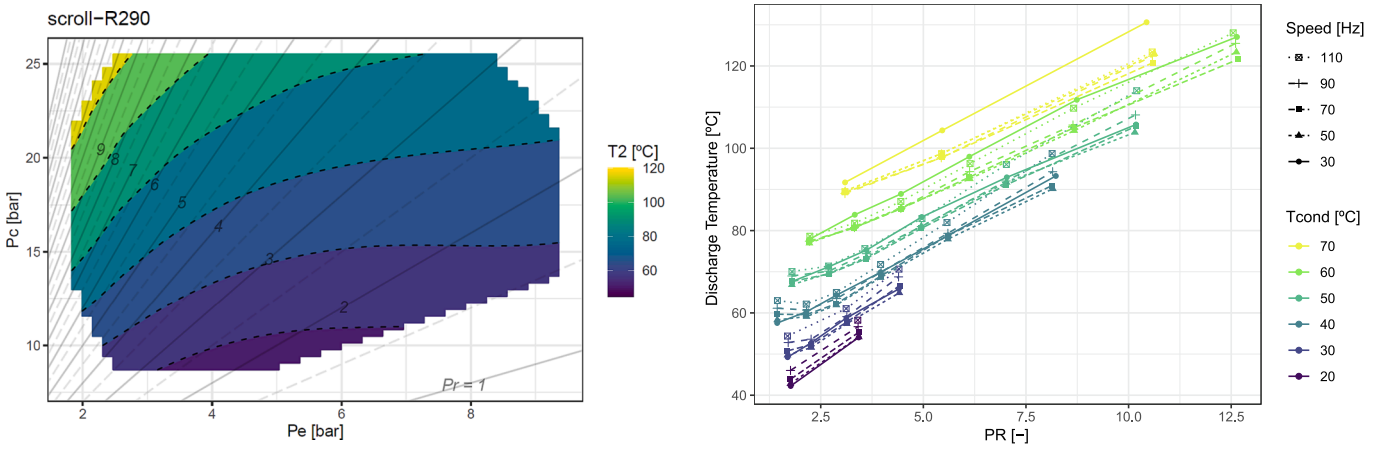

Fig. 13. Discharge temperature as a function of working pressures for nominal speed (LEFT). Discharge temperatures as a function of pressure ratio, compressor speed and condensing temperature (RIGHT).

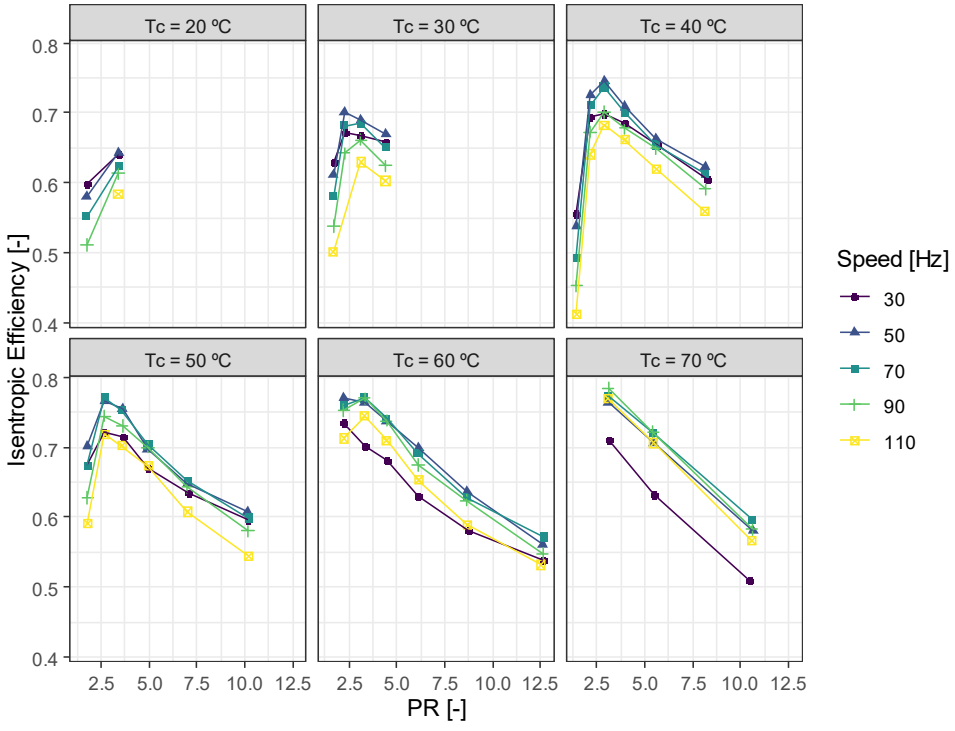

Fig. 14. Isentropic efficiency as a function of RP, compressor speed and condensing temperatures.

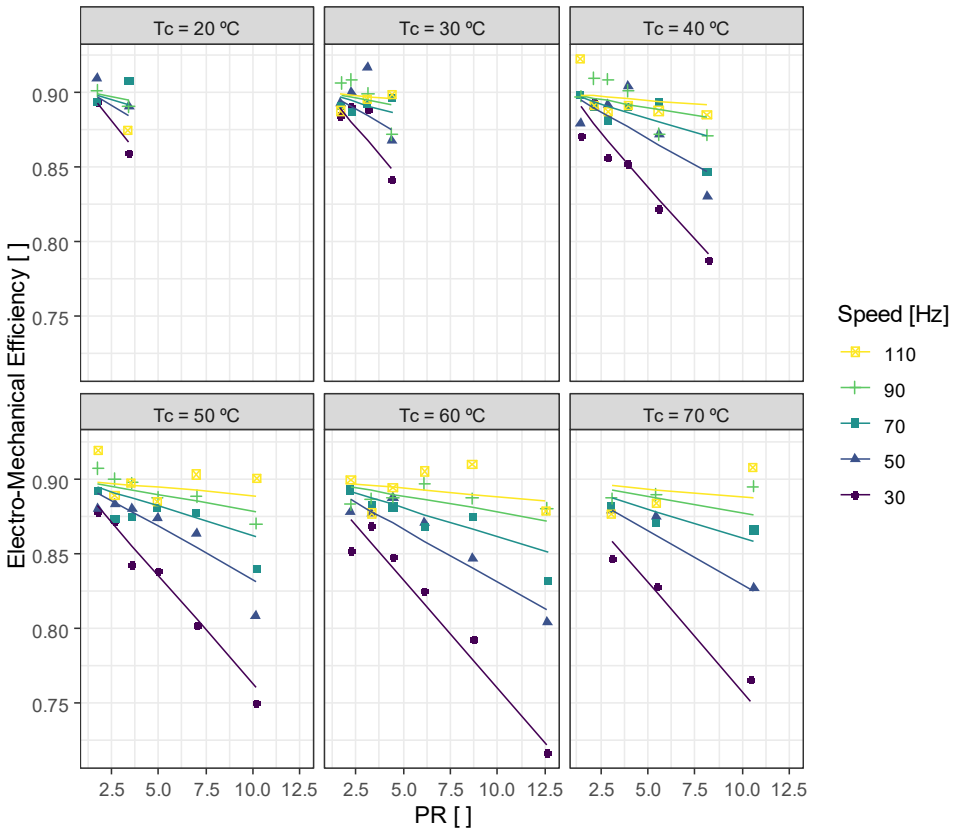

Fig. 15. Evolution of Electro-Mechanical efficiency with pressure ratio, condensing temperature and speed. Lines represent proposed model predictions.

compressors in the dataset and the obtained results are displayed in Fig. 17, together with the fitting performance of the reference Toolkit model [11].

From the results in Fig. 17 the studied compressors can be separated into two different groups: one that shows a significant modeling improvement when *PR* and f_c are considered and other that does not. The grouping does not correlate with the compression technology and could be related to dispersion in the empirical results, tested range or another non-studied factor.

In Table 5, all the proposed model's fitted coefficients [Eq.(22)] are displayed for the different compressor data sets. k_0 represents the base percentage of the compressor consumption that is lost as ambient heat and for the reference compressor is close to 10 %.

3.4. Effect of suction conditions

This section describes how to modify the presented models to account for a change in the vapor superheat temperature.

Regarding refrigerant mass flow and compressor consumption, extensive research is available in the literature. For refrigerant **mass flow**, Dabiri and Rice[21] correlation is proposed to correct the effect of suction conditions. Its formulation is displayed in Eq.(23).

$$\dot{m} = \dot{m}^{\#}\left(1 + F\left(\frac{\rho_{suc}}{\rho^{\#}_{suc}} - 1\right)\right) \tag{23}$$

Regarding $\dot{m}^{\#}$ it represents the mass flow at a rated suction conditions whose correlation is given in Eq.(10). The *F* parameter introduced in the expression can be assumed to be 0.75, value that has been generally used in the literature. However, if extra accuracy is needed and datasets at different superheats are available the parameter *F* can be fitted using experimental data.

The literature also mentions that **compressor consumption** tends to

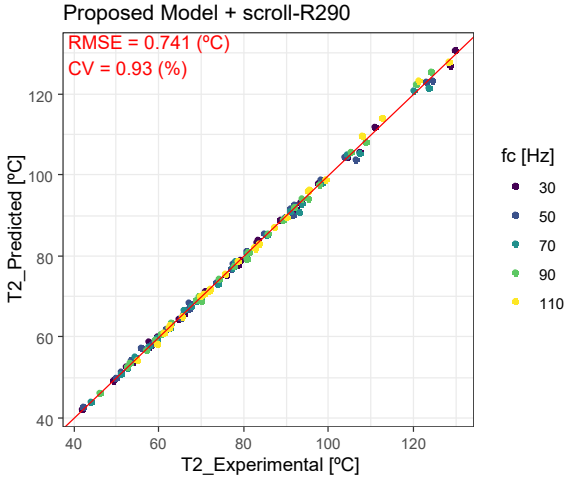

Fig. 16. Correlation plot of discharge temperature model applied to reference compressor.

be relatively unaffected by suction conditions, and the impact of superheat on consumption is usually disregarded. Consequently, Eq.(24) can be applied directly with $\dot{W}^{\#}_{esp}$ being the specific consumption obtained at rated suction conditions in Eq.(17) and $\dot{m}^{\#}$ the mass flow at the same suction conditions at which the coefficients in Eq.(17) were adjusted.

$$\dot{W}_c = \dot{W}^{\#}_c = \dot{W}^{\#}_{esp}\dot{m}^{\#} \tag{24}$$

As mentioned in the previous section, suction conditions greatly affect **discharge temperatures**, and that is why its modeling was based on

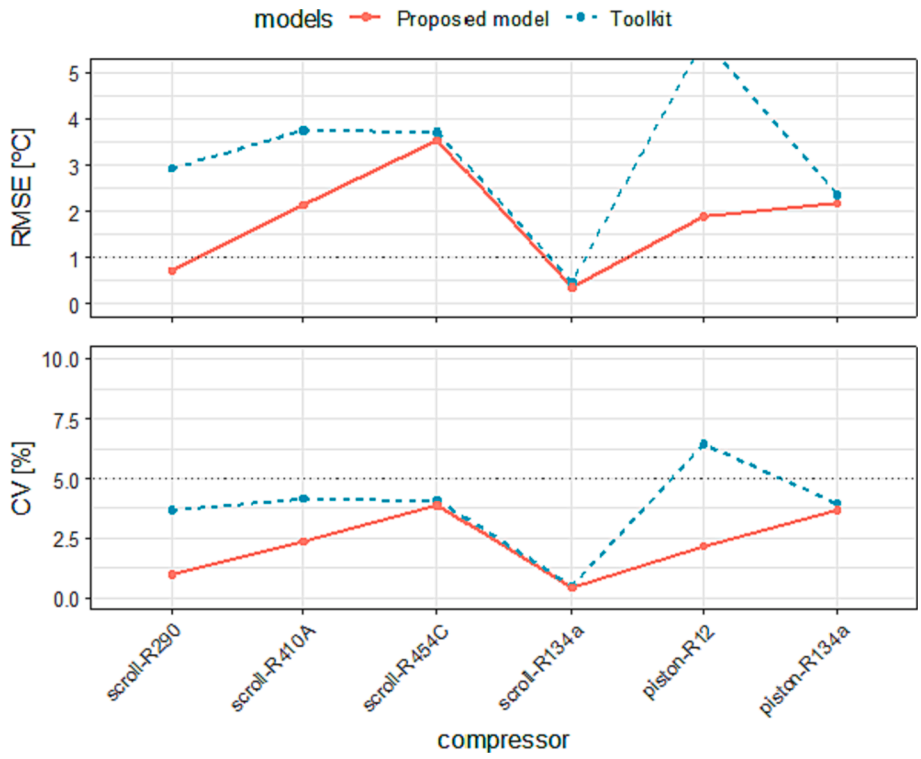

Fig. 17. Goodness of fit of discharge temperature models applied to different data sets.

Table 5
Model coefficients and goodness of fit of the proposed discharge temperature model applied to the different compressor data sets.

	scroll-R290	scroll-R410A	scroll-R454C	scroll-R134a	piston-R12	piston-R134a
k0	1.03e−01***	1.30e−02	2.75e−01***	8.45e−02***	1.29e−01***	3.10e−01+
k1	−3.90e−03***	6.34e−04	−1.86e−02+	−2.69e−02***	−3.24e−03	−5.76e−02
k2	8.00e−03***	1.31e−02***	6.97e−03	1.89e−02***	3.40e−02**	4.36e−02+
k3	−1.48e + 01**	−3.63e + 01	−1.59e + 02**	9.27e + 00	−1.40e + 01	−1.39e + 02*
Num.Obs.	133	35	87	48	25	43
RMSE	0.01	0.03	0.09	0.01	0.03	0.06
CV	1.31	3.10	10.47	1.48	3.95	6.82

electro-mechanical efficiencies (dimentionless) rather than on working temperatures. Considering $\eta^{\#}_{em}$ as the electro-mechanical efficiency at a reference suction condition, the ratio expressed in Eq.(25) can be written as:

$$\frac{\eta_{em}}{\eta^{\#}_{em}} = \frac{\dot{m}}{\dot{m}^{\#}} \frac{\dot{W}^{\#}_{c}}{\dot{W}_{c}} \frac{\Delta h}{\Delta h^{\#}} \tag{25}$$

Then, if it is supposed that consumption and enthalpy difference are not affected by the suction conditions, the proposed ratio can be simplified as a ratio of mass flows, which in turn can be approximated by Dabiri and Rice correlationin Eq.(23), resulting in the general expression for different suction conditions displayed in Eq.(26).

$$\eta_{em} = \eta^{\#}_{em} \frac{\dot{m}}{\dot{m}^{\#}} = \left(k_0 + k_1 PR + k_2 \frac{PR}{f_{c,rat}} + k_3 \frac{1}{\dot{W}_c}\right)\left(1 + F\left(\frac{\rho_{suc}}{\rho^{\#}_{suc}} - 1\right)\right) \tag{26}$$

This general correlation was tested with the dataset summarized in Table 2, consisting of a fixed-speed scroll compressor working with different refrigerants. Each refrigerant was tested at three suction conditions (SH = 11 K, SH = 22 K and T1 = 18 °C). First, the electro-mechanical model was fitted with the dataset at SH = 11 K and then it was used to predict discharge temperatures for the other suction conditions without using any correction - Fig. 18 (Left) - and using the Dabiri and Rice correction with $F = 0.75$ – Fig. 18 (Right) –.

The results in Fig. 18 show that the correction effectively reduces the prediction errors when the model is extrapolated to different suction conditions. For the particular case shown in Fig. 18 Dabiri and Rice correction reduced the prediction RMSE from 2.7 °C to values lower than 1 °C without introducing any further fitting parameters. To confirm that this result can be generalized, the same methodology was applied to the rest of the tested refrigerants and the results are summarized in Table 6.

With all the tested refrigerants, the correction significantly decreased the prediction errors of the discharge temperature without introducing new fitting parameters.

3.5. Robustness analysis

As introduced in the first section, when fitting empirical models, a recurrent problem is overfitting, which occurs when the complexity of the model is higher than the information imbibed in the data. When overfitting occurs, the model seems to fit well the train set but will fail to predict new data. To test the model against overfitting a train-test methodology is needed in which the data set is split into two groups; one will be used to fit the model coefficients and then the complete

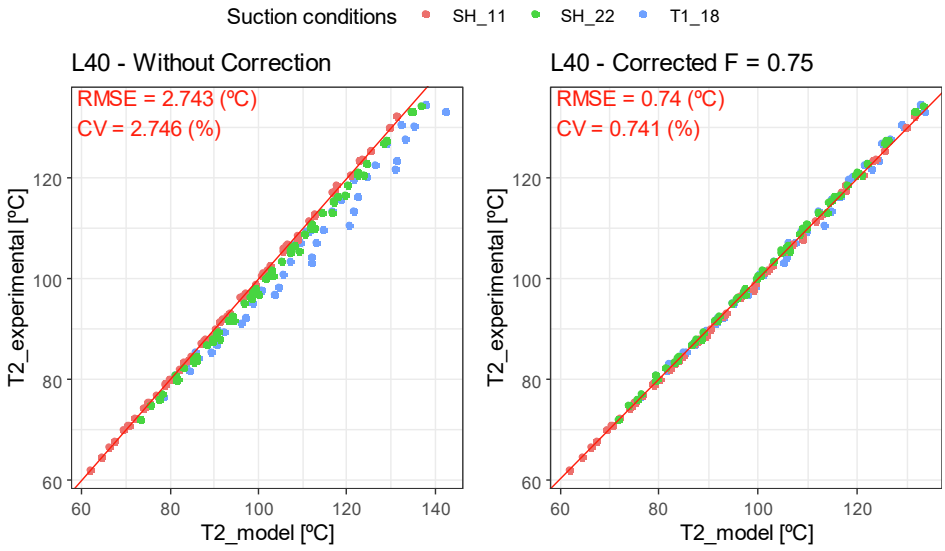

Fig. 18. Discharge temperature correlation graphs. Without correction (LEFT). Using the correction term with F = 0.75.

Table 6
Improvement of prediction errors when Dabiri correction is implemented.

Refr	No corrected		Corrected ($F = 0.75$)	
	RMSE [K]	**CV [%]**	**RMSE [K]**	**CV [%]**
R404A	1.66	2.03	0.92	1.12
ARM31a	2.46	2.58	0.70	0.73
D2Y65	2.21	2.32	0.80	0.84
L40	2.74	2.75	0.74	0.74
R32_R134a	2.74	2.61	0.91	0.87

dataset is used to check the accuracy of new predictions.

This train-test procedure was applied to both AHRI-20 model and the new proposed models to study the minimum number of tests required to fit a model avoiding overfitting.

The train-test methodology was applied 50 different times to each model and dataset. 50 different prediction errors were computed for each case which are represented aggregated using box-whiskers diagrams in Fig. 19.

For selecting the position of the train tests different methodologies arise. The simplest one is choosing the train samples randomly, however this methodology does not map the complete working range homogeneously. Clustering techniques solve this problem but tend to exclude train samples located in the borders of the working range, forcing the models to make extrapolations.

To ensure comprehensive coverage of the complete working range, including its limits, *maxDissim* methodology was selected [22]. It involves adding train tests iteratively trying to that maximize the dissimilarity between the new added samples and the existing ones. Additionally, this technique can ensure obtaining 50 different train sets by selecting each time a differernt first seed of three tests. It is important to note that the train sets selected were the same for the evaluation of both models, so a poorly train set choice would affect the performance of both tested models. Other sampling techniques, such as fully random or clustering were tested but tended to penalize AHRI-20 model more aggressively as they introduced more important extrapolations.

When less than 20 observations were selected, the AHRI-20 model was truncated, discarding high-order terms to check whether a simplified AHRI-like model could compete in accuracy with the proposed model.

Fig. 19 shows that, on average, the proposed mass flow model performed more accurately when fitted with 7 samples compared with AHRI-20 fitted with 20 samples. Additionally, Fig. 19 shows that increasing the fitting sample above 10 observations does not further improve the accuracy of the proposed model for the studied dataset. In turn, the AHRI-20 model needs to reach 25 samples to avoid overfitting and reach accuracy values similar to those obtained by the proposed model. Finally, from Fig. 19, it can also be concluded that the proposed model has better accuracy than a scaled-down AHRI-20.

Fig. 20 shows that the proposed consumption model also reaches a good accuracy with 10–15 distributed samples, but on the contrary AHRI-20 needs 25. The proposed model trained with only 10 samples performs comparable to AHRI-20 fitted with 20, and the proposed model works better than a truncated AHRI-20 model for low train sample conditions. Finally, AHRI-20 starts giving more accurate predictions for train sets with more than 25 tests for some compressors, so the latter would be preferred if a high amount of train data is available for the studied case. However, in the rotary-R22 and piston-R134a datasets, even with a high number of train samples, AHRI-20 does not manage to outperform the proposed model.

It should be remarked though, that the reported training samples were chosen trying to homogeneously map the complete compressor envelope using a smart *maxDissim* methodology so extrapolations were limited. However, the train data cannot always be gathered following a well-designed methodology, and, in those cases, models with an elevated number of coefficients could incur much higher prediction errors.

To exemplify this, Fig. 21 shows the result of adjusting AHRI-20 and the proposed model with 20 random training points. In the figure, the training tests are highlighted as black dots (and were the same for both models), the compressor envelope with the original experimental results are plotted as a solid surface (with one color for each speed), and finally the model predictions are displayed as semi-transparent meshes. It should be noted that the prediction area was deliberatively chosen to be larger than the original envelope to analyze the extrapolation capabilities of the studied models.

In Fig. 21a it can be clearly seen how the prediction surfaces of the fitted AHRI-20 model present a non-homogenous behavior that is not observed in the experimental data. In fact, even negative energy consumptions are predicted when extrapolating at low-pressure ratios. This non-desired behavior is typical of overfitted models that predict well the training data (in this case with zero prediction error as the number of coefficients matches the number of training samples) but fail to model the general behavior of the studied system (obtaining in the displayed

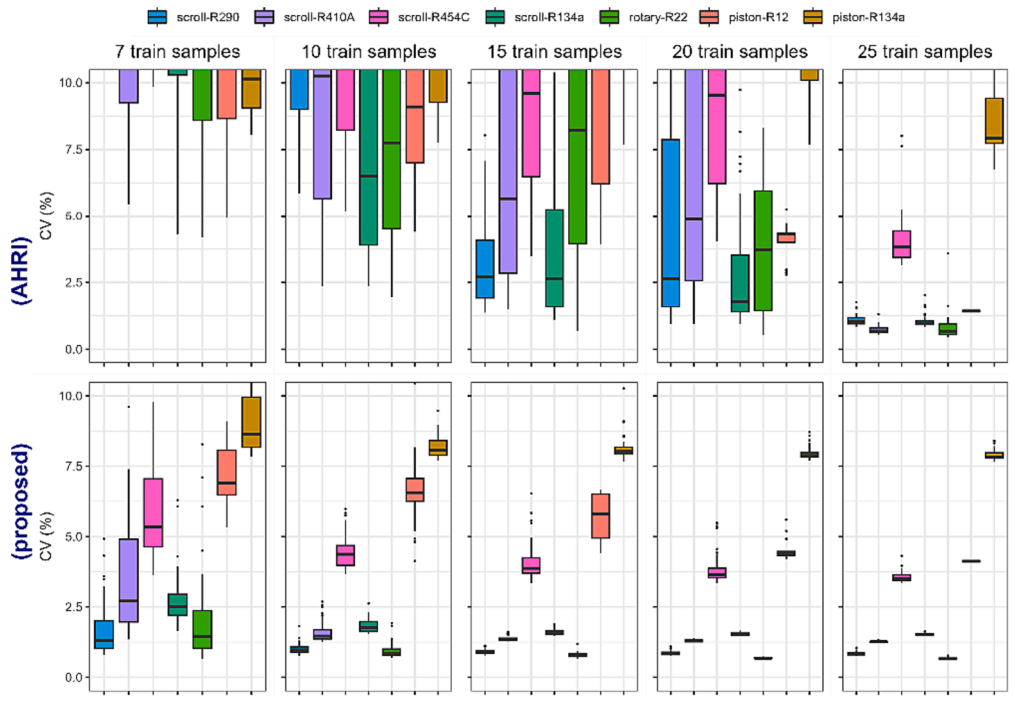

Fig. 19. Train-Test methodology to evaluate the robustness of the studied mass flow models.

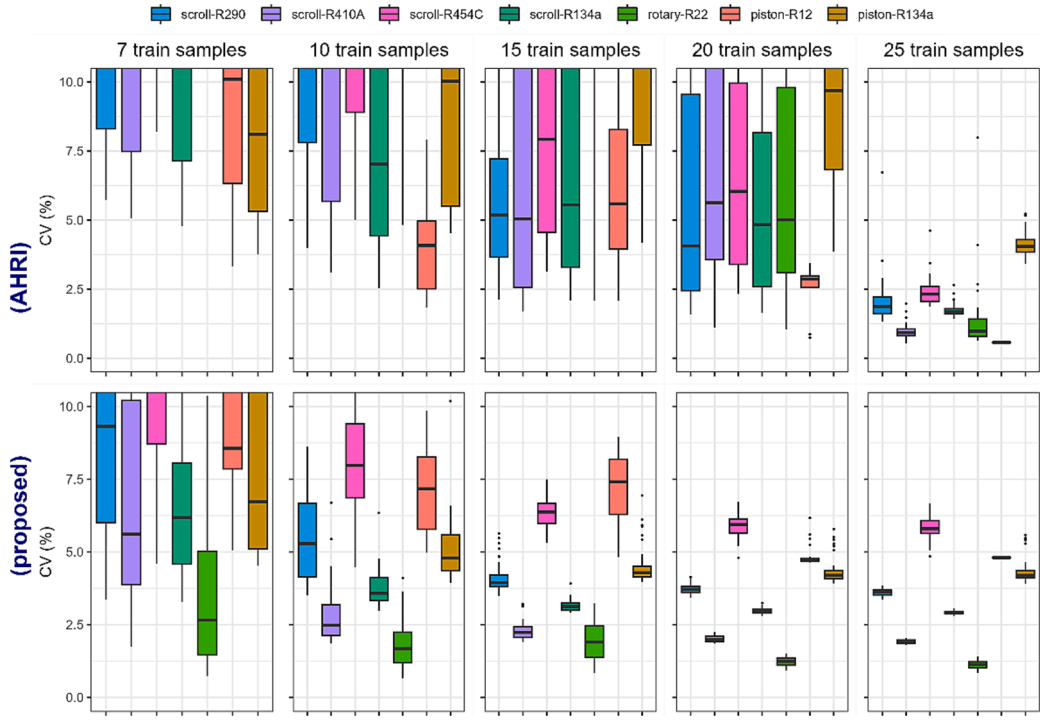

Fig. 20. Train-Test methodology to evaluate the robustness of the studied consumption models.

case a CV of 35 %). On the contrary, Fig. 21b shows the predictions of the proposed model, which faithfully reproduces the observed empirical results and manages to extrapolate the predictions outside the original tested range.

To check that the obtained results can be generalized, 100 different random sets were selected and the prediction errors were calculated for each of them. The average obtained CV was 33.7 % for the AHRI-20 model and more than 20 runs resulted in an even worse performance than the displayed in Fig. 21a. On the other hand, the proposed model obtained more consistent results (average CV of 5 %).

The obtained results outline the limitations of the AHRI-20 model to perform extrapolations (negative predictions at low pressure ratios) and also interpolations (non-physical behavior in the prediction surfaces even between train tests) when the training data is small. On the contrary, the proposed model was proven to be robust and provides reasonable extrapolation and interpolation capabilities. This can be

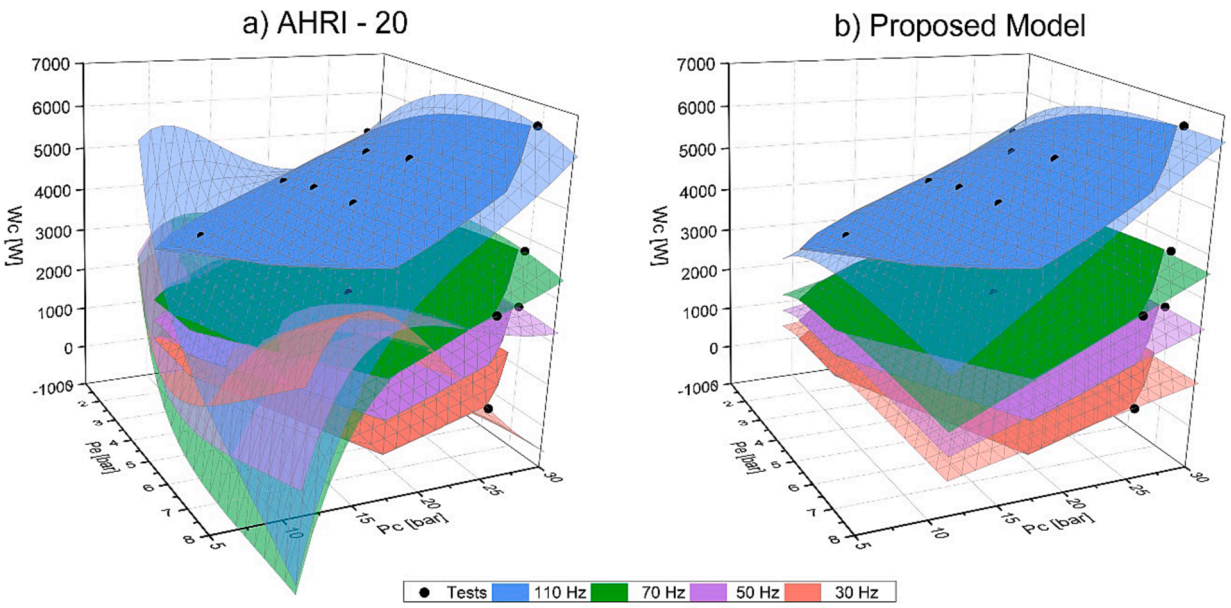

Fig. 21. Comparation between model predictions. Models were fitted using 20 tests distributed randomly. a) AHRI-20 predictions b) Proposed model predictions.

explained by the reduction of the number of model coefficients, which makes the correlation less sensitive to the position of the train data.

Given the results, in the case of using AHRI-20 model, it is highly recommended to fit its coefficients with a high number of training data and also well distributed in the response surface. Additionally, no extrapolations are recommended as the third-order terms present in the AHRI-20 correlation can create model instabilities outside the tested area.

4. Conclusions

Analyzing the performance of variable-speed compressors presents a significant challenge due to the extensive data requirements, which may explain the limited availability of published data on the subject. This study conducted an exhaustive analysis of a high-fidelity calorimetric dataset of a variable-speed compressor. The observed tendencies were crucial to designing data-driven empirical correlations using no more than six coefficients to predict mass flow, consumption and discharge temperatures. The obtained models were validated with other published datasets and the following conclusions arise:

- Mass flow
  - o A correlation with four coefficients is proposed
  - o Correlating mass flow as a function of saturating pressures, rather than temperatures, is preferred due to the resulting linear relationship.
  - o Compressor speed affects volumetric efficiency, which is modeled with a quadratic expression, adding two more fitting coefficients.
- Consumption
  - o A correlation with four coefficients is proposed.
  - o Correlating specific consumption, rather than base consumption, is favored as it partially filters the speed effect by dividing it by the refrigerant mass flow.
  - o If higher precisions is needed at extreme speeds a quadratic expression is proposed to consider the speed effect on compressor efficiency.
- Discharge temperature,
  - o the chosen modeled variable was the electro-mechanical efficiency, which was correlated using four coefficients dependent on pressure ratios and compressor speed.
- All the proposed models were generalized for changing suction conditions without adding additional coefficients to be fitted.
- Finally, a robustness analysis concluded that the proposed models are preferable to models with many coefficients, especially when the amount and quality of the empirical data is scarce and extrapolations are needed. A set of 15 tests is enough to adjust the coefficients of the proposed model. However, a model with 20 coefficients would require a minimum of 25.

In conclusion, the insights gained from this study and the robust models developed offer a practical approach to enhance the accuracy and efficiency of variable-speed compressor performance predictions. These findings contribute to the advancement of compressor technology, providing essential tools for design, selection, control, and fault detection in HVAC systems.

CRediT authorship contribution statement

Rubén Ossorio: Conceptualization, Data curation, Formal analysis, Investigation, Methodology, Software, Validation, Visualization, Writing – original draft, Writing – review & editing. **Javier Marchante-Avellaneda:** Conceptualization, Software, Supervision, Visualization, Writing – review & editing. **Emilio Navarro-Peris:** Conceptualization, Supervision.

Declaration of competing interest

The authors declare that they have no known competing financial interests or personal relationships that could have appeared to influence the work reported in this paper.

Data availability

Data will be made available on request.

Appendix 1. Electro-mechanical losses

This appendix studies in depth the influence of working variables on electro-mechanical efficiency and serves as a justification for the electro-mechanical efficiency correlation proposed in Eq.(22).

The study starts with a reformulation ASHRAE expression of electro-mechanical efficiency in which $W_{loss,0}$ is the no-load power loss and α is defined as the specific power losses (the fraction of total consumption that is lost as ambient heat [Eq.(27)]:

$$\eta_{em} = 1 - \alpha - \frac{\dot{W}_{loss,0}}{\dot{W}_c}$$

$$\text{with } \alpha = \frac{\dot{W}_{loss}}{\dot{W}_c} = \frac{\dot{W}_c - m(h_2 - h_1)}{\dot{W}_c} \tag{27}$$

In Fig. A the evolution of specific power losses (α) with the working conditions is plotted:

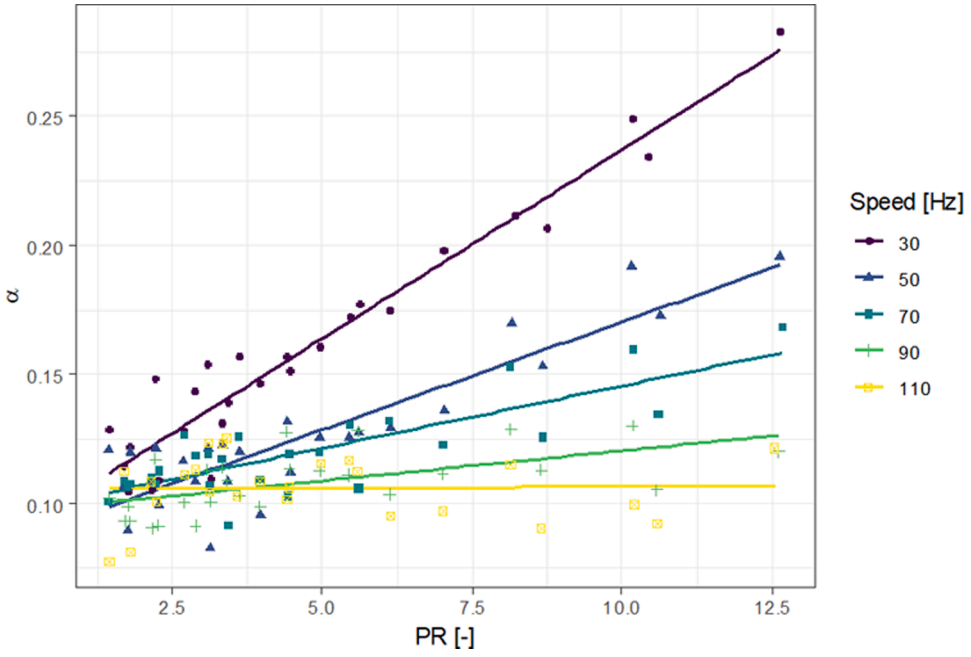

Fig. A. Evolution of specific losses as a function of pressure ratio and speed.

Fig. A shows a clear dependence of α with PR which can be modeled with a linear equation as Eq.(28).

$$\alpha = \alpha_0 - k_1 PR \tag{28}$$

According to the given formulation k_1 represents the effect of PR in specific losses and the experimental values of k_1 are plotted in Fig. B.

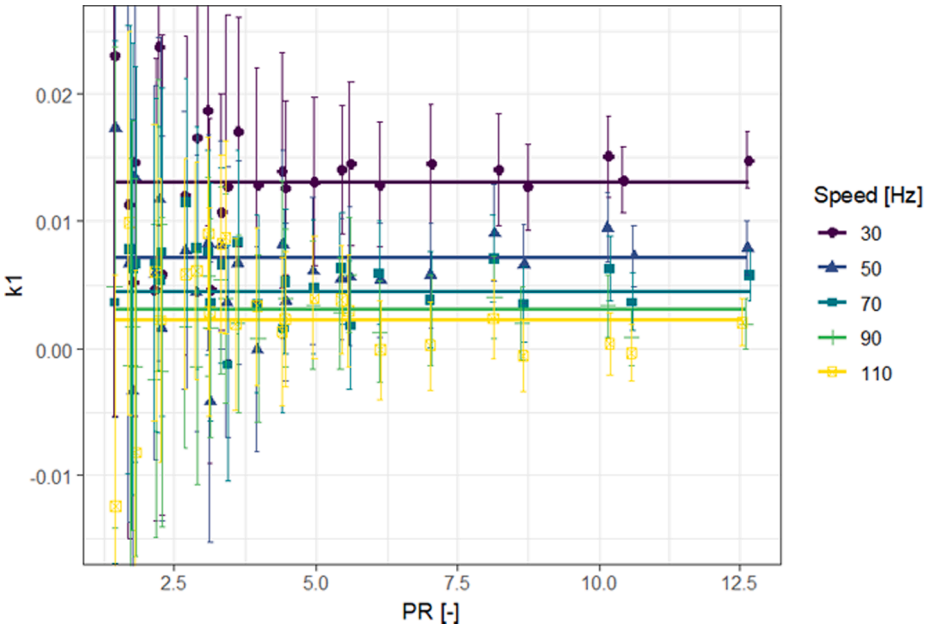

Fig. B. Evolution of k_1 as a function of pressure ratio and speed.

Fig. B shows high data dispersion at low *PR* which can be explained by empirical error, specially by the power meter uncertainty (check the uncertainty bars). On the other hand, at medium and high *PR* the empirical uncertainty decreases allowing the study of the effect of speed in k_1: at low speeds the effect of *PR* in specific losses is high and tends assimptotically to zero as speed reduces. This effect can be modeled with the correlation in Eq.(29) whose predictions are displayed in Fig. B with solid lines.

$$k_1 = k_{10} + k_{11}\frac{1}{f_{c,rat}} \tag{29}$$

Once the effect of the different variables in compressor losses has been analyzed, Eq.(27), Eq.(28) and Eq.(28) can be fusion into a final correlation for η_{em} [Eq. (30)] from where Eq.(22) is deduced.

$$\eta_{em} = \left(1 - k_0 - \left(k_1 + k_2\frac{1}{f_{c,rat}}\right)RP\right) - \frac{W_{loss,0}}{\dot{W}_c} \tag{30}$$

Appendix A. Supplementary data

Supplementary data to this article can be found online at https://doi.org/10.1016/j.applthermaleng.2024.122666.

References

[1] AHRI_540, AHRI Standard 540: Performance rating of positive displacement refrigerant compressors, 2020.
[2] Select Online, n.d. https://selectonline.emersonclimate.eu/SelectOnline/main (accessed September 9, 2022).
[3] Coolselector, n.d. https://coolselectoronline.danfoss.com/ (accessed May 17, 2022).
[4] Y. Guo, G. Li, H. Chen, Y. Hu, L. Shen, H. Li, M. Hu, J. Li, Développement d'un capteur de puissance de compresseur virtuel à vitesse variable pour un système de conditionnement d'air à débit de frigorigène variable, Int. J. Refrig. 74 (2017) 71–83, https://doi.org/10.1016/j.ijrefrig.2016.09.025.
[5] H. Wan, T. Cao, Y. Hwang, S.-D. Chang, Y.-J. Yoon, Machine-learning-based compressor models: A case study for variable refrigerant flow systems, Int. J. Refrig. 123 (2021) 23–33, https://doi.org/10.1016/j.ijrefrig.2020.12.003.
[6] R. Ossorio, E. Navarro, Testing of Variable-Speed Scroll Compressors and their inverters for the evaluation of compact energy consumption models, Appl. Therm. Eng. 230 (2023) 120725, https://doi.org/10.1016/j.applthermaleng.2023.120725.
[7] O. Ekren, S. Sahin, Y. Isler, Comparison of different controllers for variable speed compressor and electronic expansion valve, Int. J. Refrig. 33 (2010) 1161–1168, https://doi.org/10.1016/j.ijrefrig.2010.05.005.
[8] J. Ma, X. Ding, W.T. Horton, D. Ziviani, Development of an automated compressor performance mapping using artificial neural network and multiple compressor technologies, Int. J. Refrig. 120 (2020) 66–80, https://doi.org/10.1016/j.ijrefrig.2020.08.001.
[9] L. Yang, L.X. Zhao, C.L. Zhang, B. Gu, Loss-efficiency model of single and variable-speed compressors using neural networks, Int. J. Refrig. 32 (2009) 1423–1432, https://doi.org/10.1016/j.ijrefrig.2009.03.006.
[10] Ö. Kizilkan, Thermodynamic analysis of variable speed refrigeration system using artificial neural networks, Expert Syst. Appl. 38 (2011) 11686–11692, https://doi.org/10.1016/j.eswa.2011.03.052.
[11] J.P.H. Bourdouxhe, M. Grodent, K.L. Silva, J.J. Lebrun, C. Saavedra, A toolkit for primary HVAC system energy calculation. Part 2: Reciprocating chiller models, (1994). https://www.osti.gov/biblio/33295 (accessed October 10, 2023).
[12] E. Winandy, C.O. Saavedra, J. Lebrun, Simplified modelling of an open-type reciprocating compressor, Int. J. Therm. Sci. 41 (2002) 183–192, https://doi.org/10.1016/S1290-0729(01)01296-0.
[13] C. Cuevas, J. Lebrun, Testing and modelling of a variable speed scroll compressor, Appl. Therm. Eng. 29 (2009) 469–478, https://doi.org/10.1016/j.applthermaleng.2008.03.016.
[14] S. Shao, W. Shi, X. Li, H. Chen, Performance representation of variable-speed compressor for inverter air conditioners based on experimental data, Int. J. Refrig. 27 (2004) 805–815, https://doi.org/10.1016/j.ijrefrig.2004.02.008.
[15] M.H. Moradi, A. Sohani, M. Zabihigivi, H. Wirbser, A comprehensive approach to find the performance map of a heat pump using experiment and soft computing methods, Energy Convers. Manag. 153 (2017) 224–242, https://doi.org/10.1016/j.enconman.2017.09.070.

[16] Som Shrestha, Vishaldeep Sharma, Omar Abdelaziz, TEST REPORT #21 Compressor Calorimeter Test of R-404A Alternatives ARM-31a, D2Y-65, L-40, and R-32/R-134a (50/50), Oak Ridge National Laboratory, TN 3783, 2013. https://info.ornl.gov/sites/publications/files/Pub42278.pdf (accessed October 17, 2023).
[17] J. Marchante-Avellaneda, J.M. Corberan, E. Navarro-Peris, S.S. Shrestha, A critical analysis of the AHRI polynomials for scroll compressor characterization, Appl. Therm. Eng. 219 (2023) 119432, https://doi.org/10.1016/j.applthermaleng.2022.119432.
[18] J. Marchante-Avellaneda, E. Navarro-Peris, J.M. Corberan, S.S. Shrestha, Analysis of map-based models for reciprocating compressors and optimum selection of rating points, Int. J. Refrig. (2023) S0140700723001524, https://doi.org/10.1016/j.ijrefrig.2023.06.002.
[19] E. Winandy, C.S.O. Saavedra, J. Lebrun, Experimental analysis and simplified modelling of a hermetic scroll refrigeration compressor, Appl. Therm. Eng. 22 (2002) 107–120, https://doi.org/10.1016/S1359-4311(01)00083-7.
[20] M.L. Huber, E.W. Lemmon, I.H. Bell, M.O. McLinden, The NIST REFPROP Database for Highly Accurate Properties of Industrially Important Fluids, Ind. Eng. Chem. Res. (2022), https://doi.org/10.1021/ACS.IECR.2C01427.
[21] A.E. Dabiri, C.K. Rice, Compressor-simulation model with corrections for the level of suction gas superheat., (1981).
[22] M. Kuhn, Building Predictive Models in R Using the caret Package, J. Stat. Softw. 28 (2008) 1–26, https://doi.org/10.18637/jss.v028.i05.